

ANALYSIS OF GAS DELIVERABILITY CURVES FOR
PREDICTING FUTURE WELL PERFORMANCE

A Thesis

by

THOMAS GARY CORBETT

Submitted to the Graduate College of
Texas A&M University
in partial fulfillment of the requirements for the degree of
MASTER OF SCIENCE


August 1985

Major Subject: Petroleum Engineering


ANALYSIS OF GAS DELIVERABILITY CURVES FOR
PREDICTING FUTURE WELL PERFORMANCE

A Thesis
by
THOMAS GARY CORBETT


Approved as to style and content by:



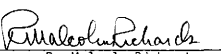
W. D. Von Gonten
(Chairman of Committee)



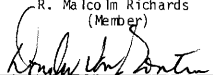
R. A. Wattenbarger
(Member)



William John Lee
(Member)



R. Malcolm Richards
(Member)



W. D. Von Gonten
(Head of Department)

August 1985

ABSTRACT

Analysis of Gas Deliverability Curves For
Predicting Future Well Performance (August 1985)

Thomas Gary Corbett, B.S., University of Texas
Chairman of Advisory Committee: Dr. W. D. Von Gonten

Transient testing techniques represent the state-of-the-art in gas well testing. However, valuable data is already available in the form of stabilized backpressure tests. A recurring problem is how to use backpressure test data to determine reservoir characteristics and predict future reservoir performance.

The commonly used deliverability equation does not adequately consider the effects of real gas behavior or non-Darcy flow. These factors cause the gas deliverability curves to deviate from the expected straight line and to shift position with time. To investigate these problems, a pseudosteady-state flow model was used to simulate backpressure tests for known reservoirs. The simulated tests were then analyzed using the techniques in the Railroad Commission of Texas (RRC) manual on backpressure testing.

The results calculated by the RRC method revealed significant errors when compared to simulated results. The RRC procedures for calculating flowing bottomhole were especially inadequate. A better

approach to analyzing backpressure tests makes use of the real gas pseudo-pressure equation for pseudosteady-state flow. This equation incorporates a non-Darcy flow term, and correctly accounts for real gas behavior. The advantages of using this equation to characterize reservoir behavior were demonstrated.

Finally, using the correct pseudo-pressure representation of the backpressure test, a simple and useful step-wise procedure of forecasting future gas well deliverability was outlined.

ACKNOWLEDGEMENTS

The author wishes to express his sincere appreciation to the following individuals:

Dr. William D. Von Gonten, Head of the Department of Petroleum Engineering, for serving as Chairman of the author's Graduate Committee and for his support.

Dr. Robert A. Wattenbarger, advisor of the author's Graduate Committee, for his patience, guidance, interest, and encouragement throughout this research.

Dr. William John Lee for serving as a member of the author's Graduate Committee and for his personal interest and support throughout the author's study at Texas A&M University.

Dr. R. Malcolm Richards for serving as a member of the author's Graduate Committee.

Mr. Scott McGregor for his help with the graphics and the manuscript.

Mr. Raymond Choo, Mr. Paul Fjerstad, Mr. Zillur Rahim, Mr. Gene Narahara, Mr. Tom Blasingame, and Mr. Joseph Olarewaju for their help, support, and friendship throughout my studies at Texas A&M University.

My parents for their love, support, and encouragement throughout my studies at Texas A&M University.

And most of all, the Lord above who gave me the strength and the will to go on when I felt like giving up.

TABLE OF CONTENTS

	page
ABSTRACT	iii
ACKNOWLEDGEMENTS	v
TABLE OF CONTENTS	vi
LIST OF TABLES	vii
LIST OF FIGURES	viii
INTRODUCTION	1
CONVENTIONAL ANALYSIS OF BACKPRESSURE TESTS	4
REAL GAS PSEUDO-PRESSURE ANALYSIS	8
RESULTS	10
Effects of Real Gas Behavior and Non-Darcy Flow	10
Shifting of Conventional Deliverability Plot	12
Downward Bending of Conventional Deliverability Plot	22
Upward Bending of Deliverability Plots	34
Effects of Bottomhole Pressure Calculation	47
Forecasting	61
DISCUSSION OF RESULTS	71
CONCLUSIONS	73
NOMENCLATURE	75
REFERENCES	78
APPENDIX A PROCEDURE FOR RUNNING BACKPRESSURE TESTS	81
APPENDIX B GENERATION OF DATA	83
APPENDIX C CORRELATIONS FOR GAS PROPERTIES	85
APPENDIX D BOTTOMHOLE PRESSURE CALCULATIONS	89
APPENDIX E FORECASTING PROCEDURE	93
VITA	99

LIST OF TABLES

Table		page
1	Properties of Hypothetical Wells	11
2	Comparison of AOF Obtained Using RRC Procedure to Actual AOF	35
3	Comparison of Deliverability Plots Without and With Non-Darcy Flow	36
4	Comparison of Bottomhole Pressures Calculated With Cullender and Smith Method and RRC Methods	49
C1	Constants for Viscosity Correlation	88

LIST OF FIGURES

Figure		page
1	Conventional Deliverability Plot	6
2	Shifting of Conventional Deliverability Plot with Declining Reservoir Pressure (Well A, without non-Darcy flow)	13
3	Shifting of Conventional Deliverability Plot with Declining Reservoir Pressure (Well B, without non-Darcy flow)	14
4	Shifting of Conventional Deliverability Plot with Declining Reservoir Pressure (Well C, without non-Darcy flow)	15
5	zu versus Pressure for Wells A, B, and C	17
6	Real Gas Pseudo-Pressure Deliverability Plot (Well A, without non-Darcy flow)	19
7	Real Gas Pseudo-Pressure Deliverability Plot (Well B, without non-Darcy flow)	20
8	Real Gas Pseudo-Pressure Deliverability Plot (Well C, without non-Darcy flow)	21
9	Downward Bending of Conventional Deliverability Plot due to Real Gas Behavior ($\bar{p} = 10,000$ psia, $\gamma_g = 0.8$, without non-Darcy flow)	23
10	Downward Bending of Conventional Deliverability Plot due to Real Gas Behavior ($\bar{p} = 5,000$ psia, $\gamma_g = 0.8$, without non-Darcy flow)	24
11	Downward Bending of Conventional Deliverability Plot due to Real Gas Behavior ($\bar{p} = 2,500$ psia, $\gamma_g = 0.8$, without non-Darcy flow)	25
12	Downward Bending of Conventional Deliverability Plot due to Real Gas Behavior ($\bar{p} = 10,000$ psia, $\gamma_g = 0.6$, without non-Darcy flow)	26
13	Downward Bending of Conventional Deliverability Plot due to Real Gas Behavior ($\bar{p} = 5,000$ psia, $\gamma_g = 0.6$, without non-Darcy flow)	27

LIST OF FIGURES (Continued)

Figure		page
14	Downward Bending of Conventional Deliverability Plot due to Real Gas Behavior ($\bar{p} = 2,500$ psia, $\gamma_g = 0.6$, without non-Darcy flow) . . .	28
15	Downward Bending of Conventional Deliverability Plot due to Real Gas Behavior ($\bar{p} = 10,000$ psia, $\gamma_g = 1.0$, without non-Darcy flow) . . .	29
16	Downward Bending of Conventional Deliverability Plot due to Real Gas Behavior ($\bar{p} = 5,000$ psia, $\gamma_g = 1.0$, without non-Darcy flow) . . .	30
17	Downward Bending of Conventional Deliverability Plot due to Real Gas Behavior ($\bar{p} = 2,500$ psia, $\gamma_g = 1.0$, without non-Darcy flow) . . .	31
18	$z\mu$ versus Pressure for Different Gas Gravities	33
19	Effect of Non-Darcy Flow on Conventional Deliverability Plot (Well B, $\bar{p} = 5,000$ psia)	38
20	Effect of Non-Darcy Flow on Real Gas Pseudo-Pressure Deliverability Plot (Well B, $\bar{p} = 5,000$ psia)	39
21	Effect of Non-Darcy Flow on Conventional Deliverability Plot (Well B, $\bar{p} = 2,500$ psia)	40
22	Effect of Non-Darcy Flow on Real Gas Pseudo-Pressure Deliverability Plot (Well B, $\bar{p} = 2,500$ psia)	41
23	Effect of Non-Darcy Flow on Conventional Deliverability Plot (Well D, $\bar{p} = 5,000$ psia)	42
24	Effect of Non-Darcy Flow on Real Gas Pseudo-Pressure Deliverability Plot (Well D, $\bar{p} = 5,000$ psia)	43
25	Effect of Non-Darcy Flow on Conventional Deliverability Plot (Well D, $\bar{p} = 2,500$ psia)	44
26	Effect of Non-Darcy Flow on Real Gas Pseudo-Pressure Deliverability Plot (Well D, $\bar{p} = 2,500$ psia)	45
27	Comparison of Backpressure Test Results Using Cullender and Smith Method and RRC Methods to Calculate Bottomhole Pressures (Well A, $\bar{p} = 1,000$ psia, without non-Darcy flow)	53

LIST OF FIGURES (Continued)

Figure		page
28	Comparison of Backpressure Test Results Using Cullender and Smith Method and RRC Methods to Calculate Bottomhole Pressures (Well A, $\bar{p} = 500$ psia, without non-Darcy flow)	54
29	Comparison of Backpressure Test Results Using Cullender and Smith Method and RRC Methods to Calculate Bottomhole Pressures (Well B, $\bar{p} = 5,000$ psia, without non-Darcy flow) . . .	55
30	Comparison of Backpressure Test Results Using Cullender and Smith Method and RRC Methods to Calculate Bottomhole Pressures (Well B, $\bar{p} = 2,500$ psia, without non-Darcy flow) . . .	56
31	Comparison of Backpressure Test Results Using Cullender and Smith Method and RRC Methods to Calculate Bottomhole Pressures (Well C, $\bar{p} = 10,000$ psia, without non-Darcy flow) . .	57
32	Comparison of Backpressure Test Results Using Cullender and Smith Method and RRC Methods to Calculate Bottomhole Pressures (Well C, $\bar{p} = 5,000$ psia, without non-Darcy flow) . . .	58
33	Comparison of Backpressure Test Results Using Cullender and Smith Method and RRC Methods to Calculate Bottomhole Pressures (Well D, $\bar{p} = 5,000$ psia, without non-Darcy flow) . . .	59
34	Comparison of Backpressure Test Results Using Cullender and Smith Method and RRC Methods to Calculate Bottomhole Pressures (Well D, $\bar{p} = 2,500$ psia, without non-Darcy flow) . . .	60
35	Forecast of Rate vs. Time for Well A (Pipeline pressure = 200 psia)	63
36	Forecast of Cum. Prod. vs. Time for Well A (Pipeline pressure = 200 psia)	64
37	Forecast of Rate vs. Time for Well B (Pipeline pressure = 1,000 psia)	65
38	Forecast of Cum. Prod. vs. Time for Well B (Pipeline pressure = 1,000 psia)	66

LIST OF FIGURES (Continued)

Figure		page
39	Forecast of Rate vs. Time for Well C (Pipeline pressure = 1,000 psia)	67
40	Forecast of Cum. Prod. vs. Time for Well C (Pipeline pressure = 1,000 psia)	68
41	Forecast of Rate vs. Time for Well D (Pipeline pressure = 1,000 psia)	69
42	Forecast of Cum. Prod. vs. Time for Well D (Pipeline pressure = 1,000 psia)	70
E1	Tubing Pressure Plot Used to Make a Forecast	94
E2	Deliverability Plot Used to Make a Forecast	95
E3	Material Balance Plot to Make a Forecast	96

INTRODUCTION

The testing of gas wells to determine their productive capabilities is an important part of the natural gas industry. Such tests are necessary for determining the commercial value of a well, determining if and when compression is needed, satisfying regulations of state agencies, designing processing plants or pipeline extensions, and forecasting performance. The types of tests performed on gas wells have evolved over the years as our understanding of reservoir and real gas behavior has increased.¹

When a pressure disturbance (caused by shutting-in or changing the rate of a well) is created in a bounded reservoir, the pressure behavior with respect to time will pass through three flow regimes, infinite acting, transition, and pseudosteady-state.² The infinite acting and transition flow regimes are characterized by a non-constant derivative of pressure with respect to time and are considered to be transient phenomena. On the other hand, the pseudosteady-state, or stabilized, flow regime is characterized by a constant derivative of pressure with respect to time throughout the entire reservoir. In gas reservoirs a true pseudosteady-state does not really exist, but a flow regime that closely resembles it does. For all practical purposes,

This thesis follows the style of the Journal of Petroleum Technology

this flow regime can be considered as pseudosteady-state.³

Techniques are available for analyzing data from both the transient and pseudosteady-state flow regimes.

In many reservoirs the time to reach pseudosteady-state conditions may be quite long. Thus, from a practical standpoint, it is desirable to stop obtaining data prior to reaching stabilized conditions. Such data can only be analyzed with transient techniques. The gathering and analysis of transient data has become quite sophisticated and today represents the state-of-the-art in gas well testing.^{4,5} However, valuable data are already available in the form of stabilized backpressure tests.

The State of Texas requires that backpressure tests be run on all gas wells for the purpose of establishing allowable production rates. The data from these tests may also be used to forecast the future productive capabilities of gas wells. From an economic and reservoir management standpoint, such a forecast is desirable. A recurring problem is how to analyze backpressure test data to obtain the best forecast possible.

The purpose of this research was to examine the common backpressure test analysis methods used today. The shortcomings of these analysis methods were investigated and compared to results obtained using better methods. Research was concentrated in three areas: 1) effects of real gas behavior and non-Darcy flow on

backpressure tests, 2) effects of bottomhole pressure calculation on backpressure tests, and 3) prediction of future reservoir performance using backpressure tests.

CONVENTIONAL ANALYSIS OF BACKPRESSURE TESTS

In 1929, the U. S. Bureau of Mines published two reports introducing the concept of backpressure testing.^{6,7} Research into the applicability of backpressure testing of gas wells continued and culminated in the publishing of the U. S. Bureau of Mines Monograph 7 by Rawlins and Schellhardt.⁸ This widely used text outlined the procedure for running and analyzing backpressure tests on gas wells.

A backpressure test is so called because it measures the ability of a gas well to produce against a constant "backpressure". The constant pressure may be a pipeline or wellhead pressure, or for analysis purposes a constant bottomhole pressure. Appendix A presents a detailed description on how a backpressure test is run.

The analysis of backpressure test data presented in Monograph 7 is based on an empirical observation that a plot of flow rate versus the difference between average reservoir pressure squared and flowing bottomhole pressure squared tends to be a straight line on log-log coordinates. The data are plotted and the "best fit" straight line is drawn through the points to obtain the deliverability plot. The equation describing the deliverability plot is:

$$q_g = C \left(\bar{p}^2 - p_{wf}^2 \right)^n \quad (1)$$

where C is a constant related to the position of the straight line plot

and n is the inverse slope of the plotted line. If the deliverability plot is extrapolated to the point corresponding to p_{wf} equal to atmospheric pressure, the absolute open flow rate (AOF) can be read. The AOF is the rate at which the well could produce if the bottomhole flowing pressure were reduced to atmospheric pressure.⁹ Fig. 1 shows the results of a typical backpressure test with the deliverability plot extrapolated to obtain the AOF. Analysis of backpressure tests employing the above empirical equation will be referred to as conventional analysis.

Meaningful results from backpressure tests using conventional analysis can only be accomplished if data from the pseudosteady-state flow regime are used.^{10,11,12} For a well centered in a finite circular reservoir, pseudosteady-state begins at $t_{DA} = 0.1$, where t_{DA} is defined as:²

$$t_{DA} = \frac{0.000264kt_s}{\phi\mu c_t(\pi r_e^2)} \quad (2)$$

Substituting in 0.1 for t_{DA} and solving for t_s gives:

$$t_s = \frac{0.1\phi\mu c_t(\pi r_e^2)}{0.000264k} \quad (3)$$

This equation can be used to estimate the time required for the reservoir to reach stabilized conditions. Although Eqs. 2 and 3 are written for a circular reservoir, they can be generalized to other reservoir shapes using the method of Dietz.¹³

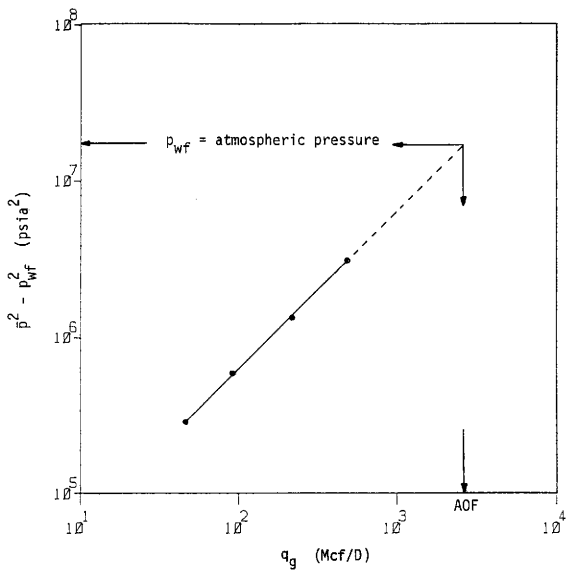


Fig. 1 - Conventional Deliverability Plot

In an effort to eliminate the need for pseudosteady-state data, many methods were developed to use transient data to predict stabilized performance.¹⁴⁻¹⁸ Most notably is the isochronal method of Cullender¹⁰ which was later modified by Katz et al..¹⁹ Many of the concepts presented in this research are applicable to isochronal testing. However, this work will concern itself only with pseudosteady-state data and conventional backpressure tests.

Although this work considers only pseudosteady-state flow, it should be mentioned that the concept of backpressure testing is also applicable to steady-state flow. Steady-state flow occurs when reservoir pressure is maintained by some outside force. This force may be a result of gas injection or a strong water drive.

REAL GAS PSEUDO-PRESSURE ANALYSIS

The methods outlined in Monograph 7 for running and analyzing backpressure tests have remained virtually unchanged to this day. However, some important technological advances that should be incorporated into the analysis of backpressure tests have been made. In 1966, Al-Hussainy, Ramey, and Crawford³ published a paper describing the real gas pseudo-pressure. The real gas pseudo-pressure, written as $m(p)$, integrates the effects of viscosity, pressure, and z -factor into a single function defined as:

$$m(p) = 2 \int_0^p \frac{p'}{z(p')\mu(p')} dp' \quad (4)$$

Wattenbarger and Ramey²⁰ verified that the use of this function in place of pressure in gas flow equations removes the necessity of defining ideal or average gas properties.

Another paper by Al-Hussainy and Ramey²¹ described a method of using the real gas pseudo-pressure to analyze backpressure tests. This method is based on the real gas equation for pseudosteady-state flow. In terms of real gas pseudo-pressure, this equation is:

$$q_g = \left[1.987 \times 10^{-5} \left(\frac{T_{sc}}{p_{sc} T} \right) \frac{kh}{\ln \frac{r_e}{r_w} + s + D(u)q_g} \right] (m(\bar{p}) - m(p_{wf})) \quad (5)$$

where $D(u)q_g$ represents the non-Darcy flow term used by Wattenbarger.²² If non-Darcy flow is negligible, a plot of q_g

versus $m(\bar{p}) - m(p_{wf})$ will be a straight line with a unit slope on log-log coordinates. Analysis of backpressure tests using the real gas pseudo-pressure will be referred to as real gas pseudo-pressure analysis. The plot of q_g versus $m(\bar{p}) - m(p_{wf})$ will be referred to as the real gas pseudo-pressure, or $m(p)$, deliverability plot to distinguish it from the conventional deliverability plot described by Eq. 1. As with conventional analysis, real gas pseudo-pressure analysis, as described above, is applicable only to data taken while the reservoir is in the pseudosteady-state flow regime. A detailed description of using the real gas pseudo-pressure to analyze backpressure tests can be found in the Theory and Practice of the Testing of Gas Wells.⁴ In the following sections, the advantages of real gas pseudo-pressure analysis over conventional analysis will be shown.

RESULTS

The results presented in the following sections are based on backpressure test data generated using Eq. 5. Data were generated on four hypothetical gas reservoirs. The reservoirs were assumed to be finite, circular, homogeneous, and isotropic with a single producing well located in the center. Relevant gas and reservoir properties are shown in Table 1. A detailed description of how the data were generated is given in Appendix B.

Effects of Real Gas Behavior and Non-Darcy Flow

To see the effects of real gas behavior and non-Darcy flow on backpressure test results, Eq. 5 can be rewritten in terms of pressure squared:

$$q_g = \left[1.987 \times 10^{-5} \left(\frac{T_{sc}}{p_{sc} T} \right) \frac{kh}{\ln \frac{0.472r}{r_w} + s + D(\mu)q_g} \left(\frac{1}{(z\mu)_{avg}} \right) \right] (\bar{p}^2 - p_{wf}^2) \quad (6)$$

Numerical simulation studies^{23,24} have shown that if $(z\mu)_{avg}$ is defined at the correct average pressure then this equation gives exactly the same results as Eq. 5. The same studies also suggest that the following average pressure be used to evaluate $(z\mu)_{avg}$:

$$p_{avg} = \frac{1}{2}(\bar{p} + p_{wf}) \quad (7)$$

Table 1 - Properties of Hypothetical Wells

	<u>Well A</u>	<u>Well B</u>	<u>Well C</u>	<u>Well D</u>
Gas gravity, fraction	0.8	0.8	0.8	0.8
Depth, ft	1,000	5,000	10,000	5,000
T , °F	100	195	310	195
p_i , psia	1,000	5,000	10,000	5,000
k , md	1	1	1	25
h , ft	10	10	10	20
ϕ , fraction	0.05	0.05	0.05	0.05
S_g , fraction	0.80	0.80	0.80	0.80
r_w , ft	0.333	0.333	0.333	0.333
r_e , ft	2,980	2,980	2,980	2,980
T_{wh} , °F	80	95	110	95
T_{sc} , °F	60	60	60	60
p_{sc} , psia	14.7	14.7	14.7	14.7
Tubing length, ft	1,000	5,000	10,000	5,000
Tubing I.D., in	2.441	2.441	2.441	2.441
Pipe roughness, in	0.0006	0.0006	0.0006	0.0006

(Unless otherwise stated, referral to Wells A, B, C and D will imply the above conditions)

Comparing Eqs. 1 and 6, it is seen that if n equals one, C in Eq. 1 is analogous to the bracketed term in Eq. 6. Thus we can define:

$$C \equiv 1.987 \times 10^{-5} \left(\frac{T_{sc}}{p_{sc} T} \right) \frac{kh}{\ln \frac{0.472r_e}{r_w} + s + D(\mu)q_g} \left(\frac{1}{(z\mu)_{avg}} \right) \quad (8)$$

Eq. 8 shows that the value of C will change as z , μ , and q_g change. This conclusion is contrary to the assumption made in conventional analysis that C is constant. The effects of a non-constant C on the conventional deliverability plot are threefold: 1) the plot will shift positions as gas properties change, 2) the plot will bend downward due to changing gas properties, and 3) the plot will bend upward if non-Darcy flow effects are significant.

Shifting of Conventional Deliverability Plot

To demonstrate how the deliverability plot will shift with changing gas properties when using conventional analysis, backpressure test data were generated on Wells A, B, and C. Average reservoir pressures equal to 100, 75, and 50 per cent of initial reservoir pressure were used. Flow rates for each test were calculated at flowing bottomhole pressures ranging from 75 to 95 per cent of the average reservoir pressure. In these tests, skin and non-Darcy flow effects were not included. Results from conventional analysis are presented in Figs. 2, 3, and 4.

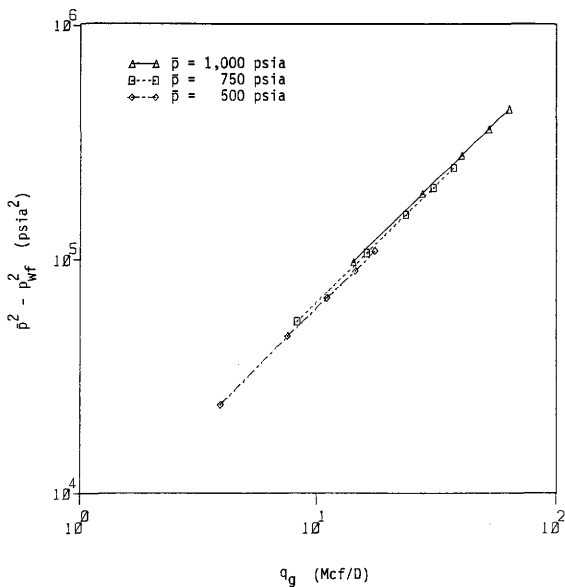


Fig. 2 - Shifting of Conventional Deliverability Plot with Declining Reservoir Pressure (Well A, without non-Darcy flow)

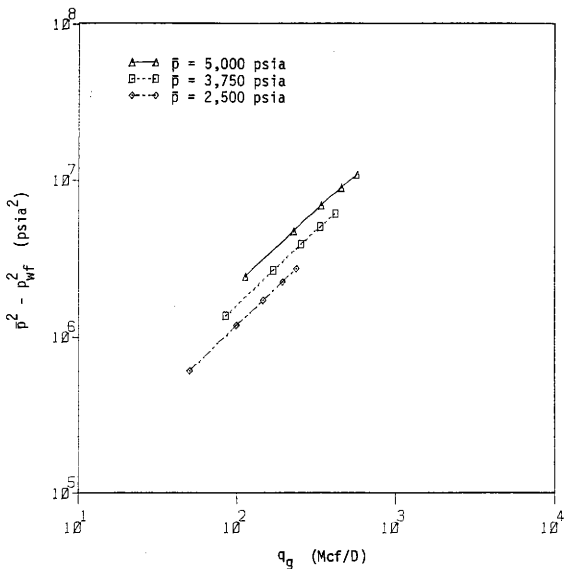


Fig. 3 - Shifting of Conventional Deliverability Plot with Declining Reservoir Pressure (Well B, without non-Darcy flow)

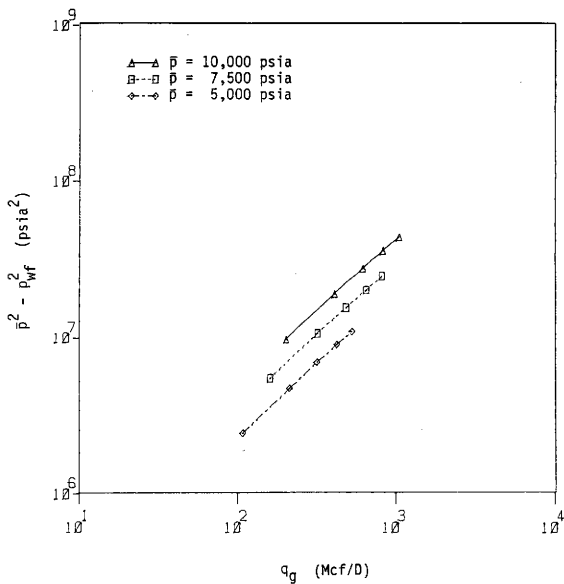


Fig. 4 - Shifting of Conventional Deliverability Plot
 with Declining Reservoir Pressure
 (Well C, without non-Darcy flow)

Two trends are noticeable when examining Figs. 2, 3, and 4. First, for a given well, as reservoir pressure is lowered, the deliverability plot shifts downward and to the left. Second, the magnitude of the downward shift becomes less for lower pressured systems (e.g., compare Figs. 2 and 4). The shift to the left is expected due to depletion of the reservoir. As the reservoir is depleted, average reservoir pressure drops. This in turn reduces the magnitude of pressure drawdown between the reservoir and the well, resulting in lower flow rates. The lower flow rates cause the plot to shift. The downward shift and the magnitude of the shift are results of changing gas properties.

Fig. 5 shows a plot of $z\mu$ versus pressure for the gases used in Wells A, B, and C. Note that the value of $z\mu$ increases slowly at low pressures and more rapidly at high pressures. Looking at Eq. 7, we can see that the pressure at which $(z\mu)_{avg}$ is calculated is influenced by the average reservoir pressure, \bar{p} . For a high \bar{p} , the pressure at which $(z\mu)_{avg}$ is calculated will also be high. As \bar{p} declines, due to reservoir depletion, the pressure at which $(z\mu)_{avg}$ is calculated will also decline. Thus, the magnitude of $(z\mu)_{avg}$ will decrease along with \bar{p} . To relate the decrease in $(z\mu)_{avg}$ to the deliverability plot, we look at Eq. 8. As $(z\mu)_{avg}$ decreases, the value of C increases. For a given flow rate, a larger value of C results in a smaller value of $\bar{p}^2 - p_{wf}^2$. This is why the deliverability plot shifts downward with declining reservoir pressure.

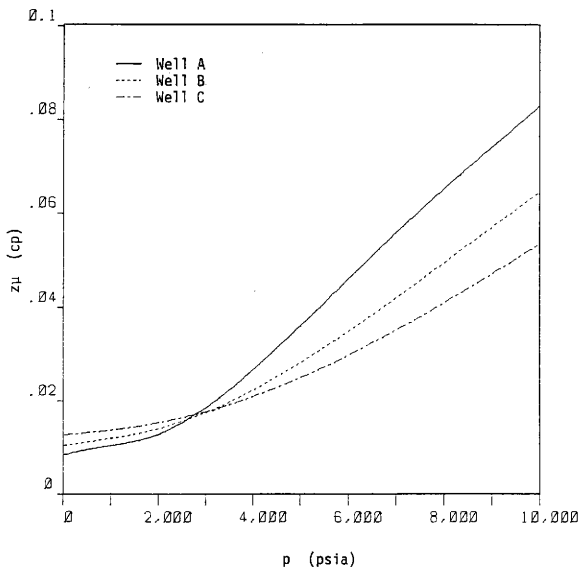


Fig. 5 - $z\mu$ versus Pressure for Wells A, B, and C

To understand why the magnitude of the shift is greater for higher pressured reservoirs, we look again at Fig. 5. For Well A, the initial reservoir pressure is 1,000 psia. A fifty per cent drop in average reservoir pressure (i.e., down to 500 psia) results in a less than five per cent change in $z\mu$. Thus for Well A, the value of C does not change appreciably and the curves on Fig. 2 lie closer together. On the other hand, for Well C, whose initial pressure is 10,000 psia, a fifty per cent change in average reservoir pressure results in a more than fifty per cent change in $z\mu$. Thus for Well C, the value of C changes significantly. The large change in C is reflected in a large shift in the deliverability plots for Well C at different average reservoir pressures.

If the backpressure tests represented in Figs. 2, 3, and 4 are analyzed using real gas pseudo-pressure, changing gas properties are properly accounted for. If this were so, and non-Darcy flow effects are negligible, we would expect a single straight line plot for all values of reservoir pressure. Figs. 6, 7, and 8 show the $m(p)$ deliverability plots corresponding to Figs. 2, 3, and 4. Examining the $m(p)$ deliverability plots indicates that all points for all tests on a given well fall on a straight line. Therefore, real gas pseudo-pressure analysis eliminates the downward shift seen in conventional deliverability plots.

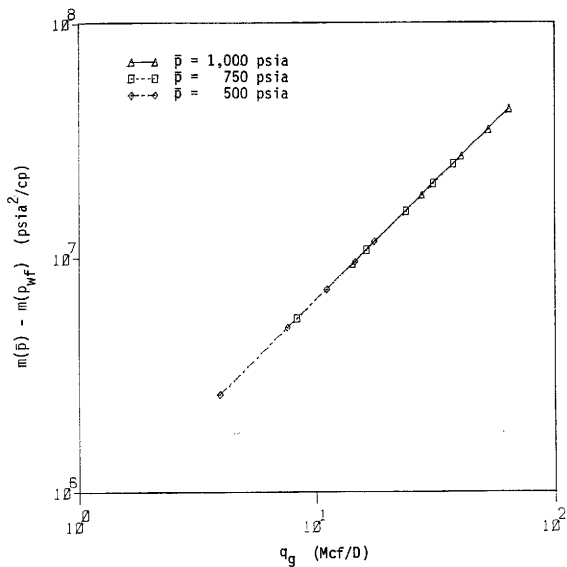


Fig. 6 - Real Gas Pseudo-Pressure Deliverability Plot
(Well A, without non-Darcy flow)

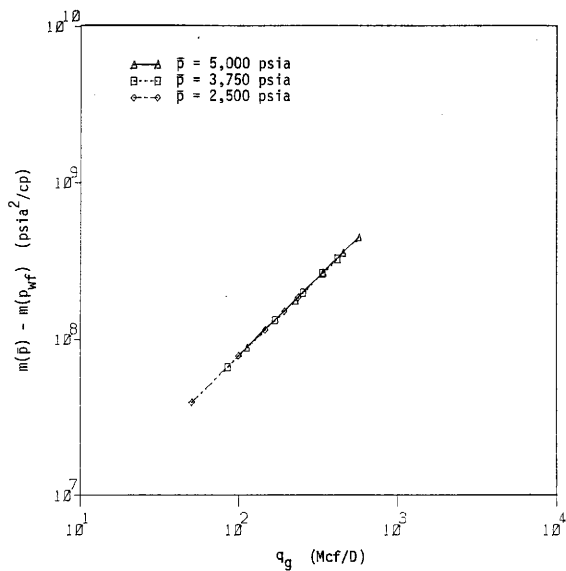


Fig. 7 - Real Gas Pseudo-Pressure Deliverability Plot
(Well B, without non-Darcy flow)

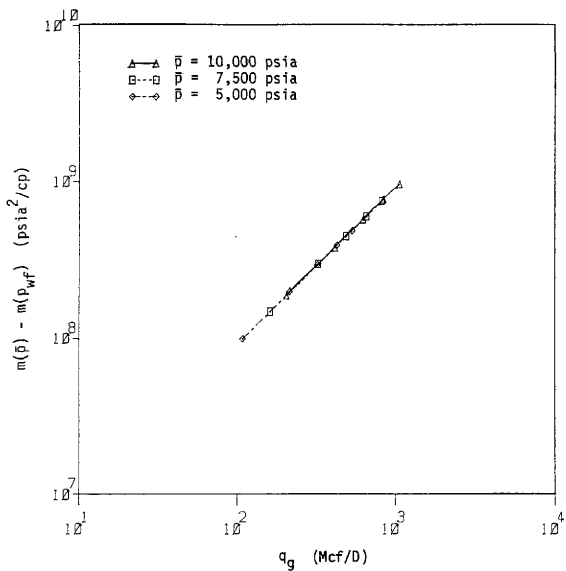


Fig. 8 - Real Gas Pseudo-Pressure Deliverability Plot
(Well C, without non-Darcy flow)

Downward Bending of Conventional Deliverability Plot

The conventional deliverability plots shown in Figs. 2, 3, and 4 appear to be straight lines. In reality, they are slightly curved. To show the bending more clearly, backpressure test results were generated for Well C (Wells A and B also exhibit curvature, but since the curvature is more pronounced at higher pressures, only Well C was considered here). Tests were done at average reservoir pressures corresponding to 100, 50, and 25 per cent of initial reservoir pressure. Flowing bottom-hole pressures ranged from 10 to 95 per cent of the average reservoir pressure. Skin effects and non-Darcy flow were not included. The tests were performed at a gas gravity of 0.8 and then repeated for gravities of 0.6 and 1.0. Results are presented in Figs. 9 through 17. Also shown on these figures is a straight line of unit slope that would result if z_u were held constant at a value corresponding to \bar{p} .

Since non-Darcy flow is neglected, the curvature in deliverability plots shown in Figs. 9 through 17 can be attributed to changing gas properties only. For the same reason changing \bar{p} caused the deliverability plots to shift, changing p_{wf} causes the deliverability plots to bend downward. The degree of curvature is determined by the difference between \bar{p} and p_{wf} . For a small difference, resulting in low flow rates, $(z_u)_{avg}$ evaluated at p_{avg} calculated with Eq. 7 will not differ appreciably from z_u calculated at \bar{p} . So, the deliverability plot will not deviate too far

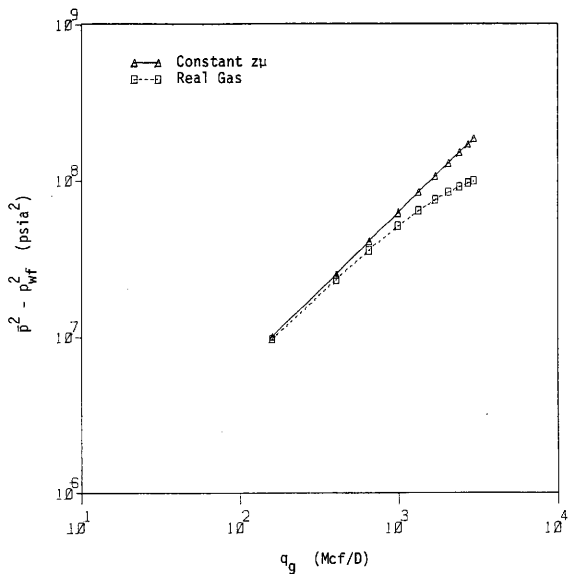


Fig. 9 - Downward Bending of Conventional Deliverability Plot due to Real Gas Behavior
 ($p = 10,000$ psia, $\gamma_g = 0.8$, without non-Darcy flow)

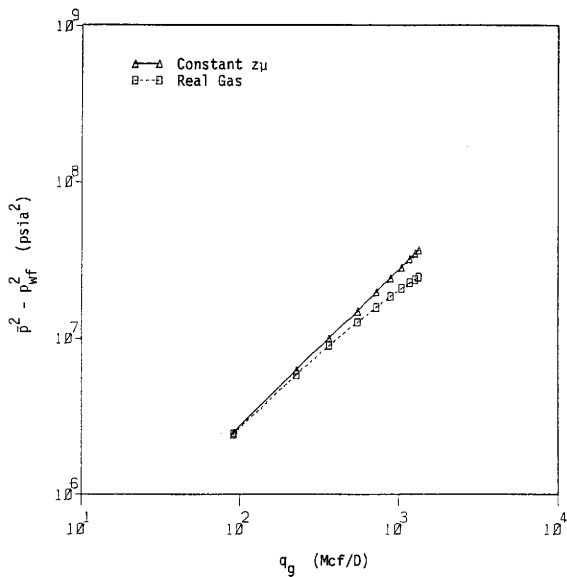


Fig. 10 - Downward Bending of Conventional Deliverability Plot due to Real Gas Behavior
 ($p = 5,000$ psia, $\gamma_g = 0.8$, without non-Darcy flow)

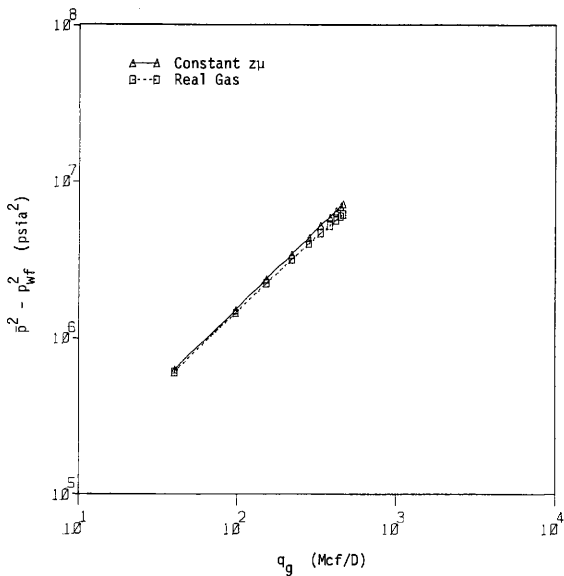


Fig. 11 - Downward Bending of Conventional Deliverability Plot due to Real Gas Behavior
 ($p = 2,500$ psia, $\gamma_g = 0.8$, without non-Darcy flow)

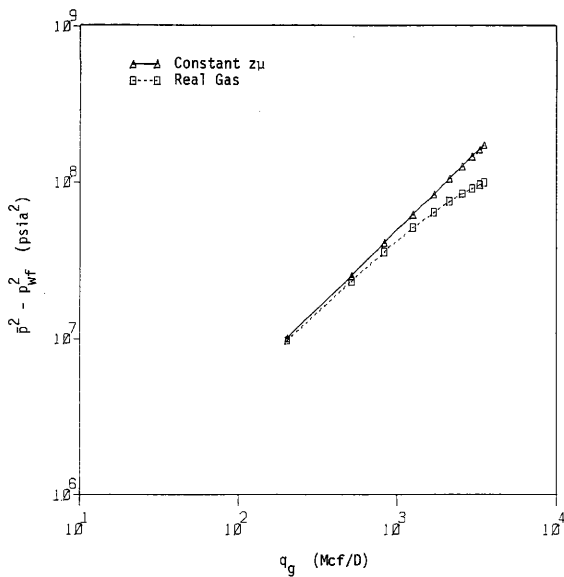


Fig. 12 - Downward Bending of Conventional Deliverability Plot due to Real Gas Behavior
 ($p = 10,000$ psia, $\gamma_g = 0.6$, without non-Darcy flow)

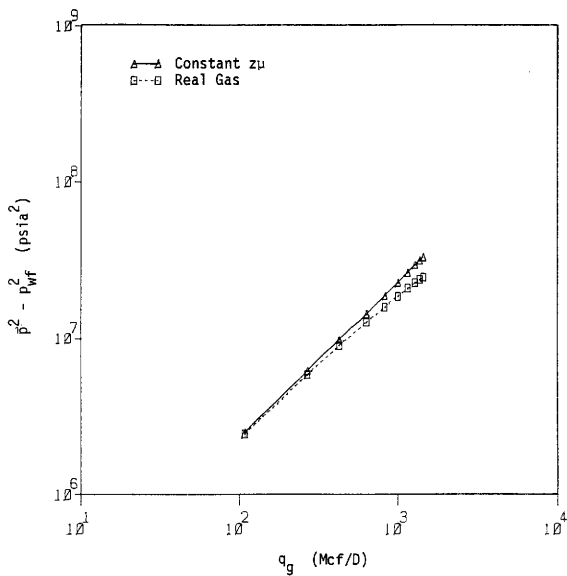


Fig. 13 - Downward Bending of Conventional Deliverability Plot due to Real Gas Behavior
 ($p = 5,000$ psia, $\gamma_g = 0.6$, without non-Darcy flow)

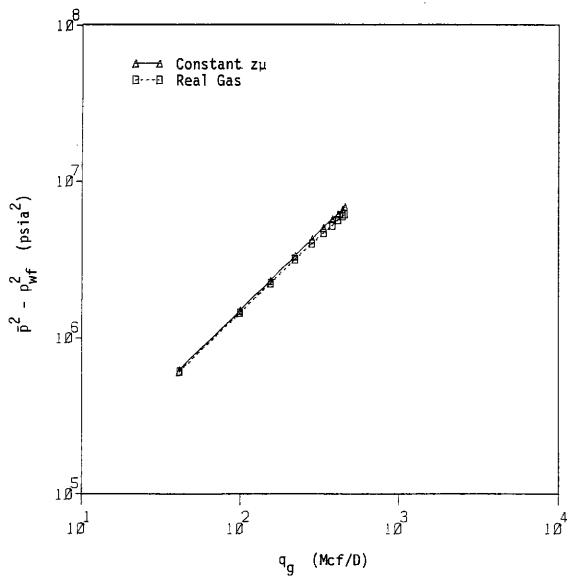


Fig. 14 - Downward Bending of Conventional Deliverability Plot due to Real Gas Behavior
 ($p = 2,500$ psia, $\gamma_g = 0.6$, without non-Darcy flow)

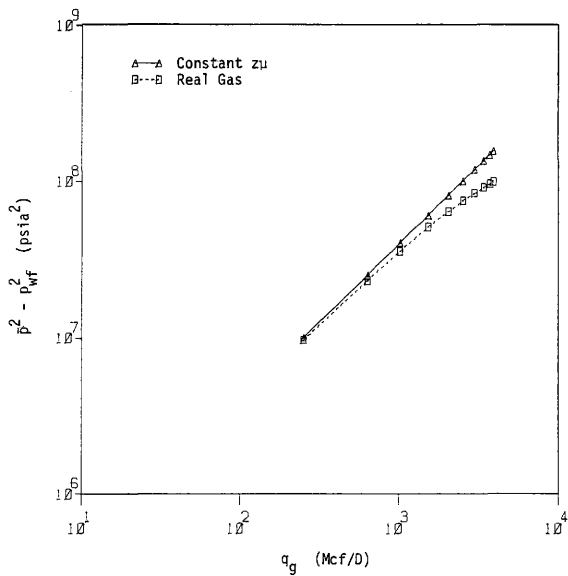


Fig. 15 - Downward Bending of Conventional Deliverability Plot due to Real Gas Behavior
 ($p = 10,000$ psia, $\gamma_g = 1.0$, without non-Darcy flow)

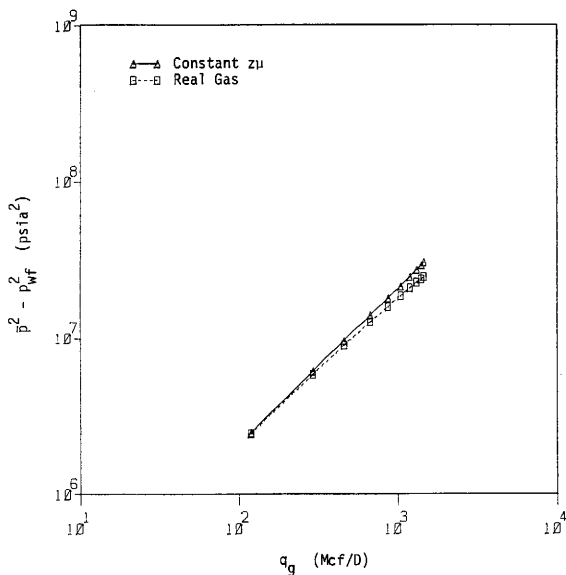


Fig. 16 - Downward Bending of Conventional Deliverability Plot due to Real Gas Behavior
 ($p = 5,000$ psia, $\gamma_g = 1.0$, without non-Darcy flow)

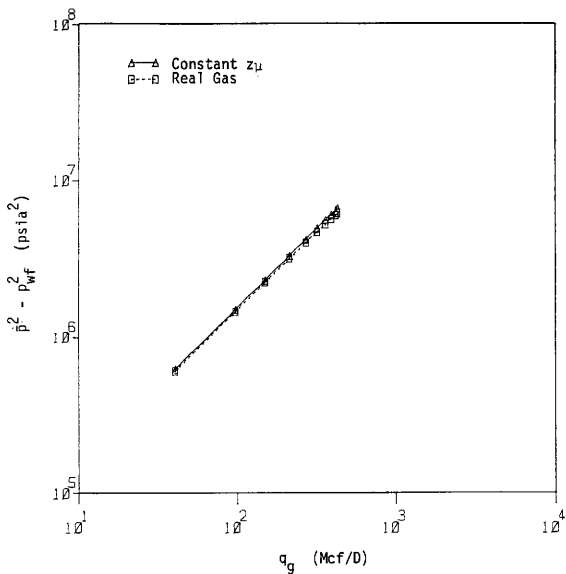


Fig. 17 - Downward Bending of Conventional Deliverability Plot due to Real Gas Behavior
 ($p = 2,500$ psia, $\gamma_g = 1.0$, without non-Darcy flow)

from the straight line. As p_{wf} is lowered, resulting in high flow rates, the difference between $(z_{\mu})_{avg}$ calculated at p_{avg} will be significantly different from z_{μ} evaluated at \bar{p} . The more significant the difference, the more the deliverability plot will deviate from the straight line.

Examining Figs. 9 through 17 indicates that the curvature in the deliverability plots increases for higher gravity gases. Fig. 18 shows a plot of z_{μ} versus pressure for gas gravities of 0.6, 0.8, and 1.0 at a temperature of 310 degrees Fahrenheit. From this plot, it is seen that as gas gravity increases, the change in z_{μ} with pressure also increases. Thus, for the same change in pressure, the magnitude of the change in z_{μ} will be greater for a gas with a gravity of 1.0 than for a gas with a gravity of 0.6. This accounts for the greater curvature observed as gas gravity increases.

As explained in Appendix A, most backpressure tests consist of data gathered at bottomhole flowing pressures corresponding to 75 to 95 per cent of average reservoir pressure. This range of data is reflected in the first four points on Figs. 9 through 17. If a straight line is drawn through the first four points, the slope of the line will be less than one. The Railroad Commission of Texas (RRC)²⁵ will not accept a backpressure test whose deliverability plot has a slope less than one. If a slope less than one does occur, the Railroad Commission requires that a unit slope straight line be drawn through the data point with the highest rate of flow. This

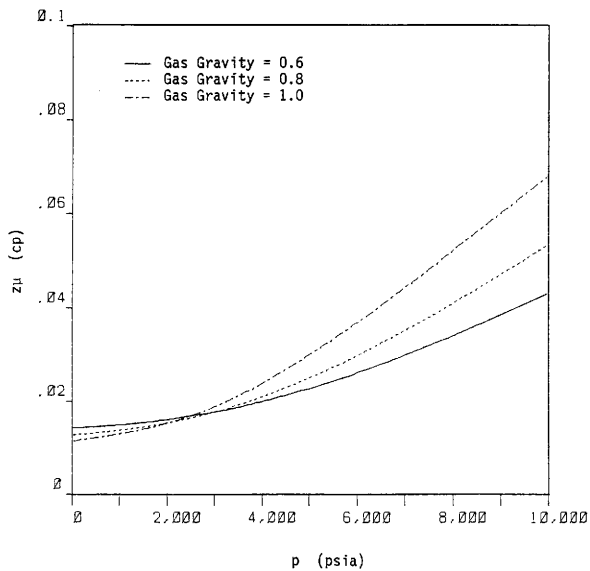


Fig. 18 - $z\mu$ versus Pressure for Different Gas Gravities

straight line is extrapolated to find the AOF. This procedure was used to calculate the AOF for the test shown in Figs. 9 through 17. The fourth data point (corresponding to p_{wf} equal to seventy-five per cent of \bar{p}) was assumed to be the data point with the highest rate of flow possible in a typical backpressure test. The absolute open flows calculated with the RRC method are compared to the actual absolute open flow rates determined from the bending line. The results of this analysis are presented in Table 2. As expected, the highest errors occur in the high pressure cases (where z_u changes most rapidly). Note also that the error increases slightly as gas gravity increases.

Upward Bending of Deliverability Plots

To investigate the effects of non-Darcy flow, backpressure tests were run on Wells B and D. These wells are identical except for permeability and thickness. Tests were done at reservoir pressures equal to 5,000 and 2,500 psia. Flowing bottomhole pressures ranged from 75 to 95 per cent of average reservoir pressure. The tests were run with and without non-Darcy flow effects. The results from the test are presented in Table 3. Figs. 19 through 26 show conventional and $m(p)$ deliverability plots.

For a given flow rate, non-Darcy flow causes a larger pressure drop between the formation and the wellbore than predicted by Darcy's law. The additional pressure drop is similar to the effects of a

Table 2 - Comparison of AOF Obtained Using
RRC Procedure to Actual AOF

For gas gravity = 1.0

<u>Average pressure (psia)</u>	<u>Correct AOF from bending line (Mcf/D)</u>	<u>AOF from RRC procedure (Mcf/D)</u>	<u>Per cent error</u>
10,000	3,075	1,957	36
5,000	1,366	1,077	21
2,500	471	435	8

For gas gravity = 0.8

<u>Average pressure (psia)</u>	<u>Correct AOF from bending line (Mcf/D)</u>	<u>AOF from RRC procedure (Mcf/D)</u>	<u>Per cent error</u>
10,000	3,611	2,488	31
5,000	1,463	1,242	15
2,500	462	437	5

For gas gravity = 0.6

<u>Average pressure (psia)</u>	<u>Correct AOF from bending line (Mcf/D)</u>	<u>AOF from RRC procedure (Mcf/D)</u>	<u>Per cent error</u>
10,000	4,025	3,019	25
5,000	1,481	1,322	11
2,500	438	423	3

Table 3 - Comparison of Deliverability Plots
Without and With Non-Darcy Flow

Well B - Average Reservoir Pressure = 5,000 psia

q_g	Without non-Darcy Flow			With non-Darcy Flow		
	p_{wf}	$\bar{p}^2 - p_{wf}^2$	$m(\bar{p}) - m(p_{wf})$	p_{wf}	$\bar{p}^2 - p_{wf}^2$	$m(\bar{p}) - m(p_{wf})$
114.1	4,750	.2438E7	.8875E8	4,749	.2451E7	.8926E8
228.7	4,500	.4750E7	.1779E9	4,494	.4804E7	.1807E9
343.7	4,250	.6938E7	.2674E9	4,235	.7056E7	.2724E9
458.8	4,000	.9000E7	.3569E9	3,974	.9207E7	.3662E9
573.6	3,750	.1094E8	.4462E9	3,707	.1125E8	.4614E9

Well B - Average Reservoir Pressure = 2,500 psia

q_g	Without non-Darcy Flow			With non-Darcy Flow		
	p_{wf}	$\bar{p}^2 - p_{wf}^2$	$m(\bar{p}) - m(p_{wf})$	p_{wf}	$\bar{p}^2 - p_{wf}^2$	$m(\bar{p}) - m(p_{wf})$
50.9	2,375	.6094E6	.3960E8	2,374	.6130E6	.3975E8
100.6	2,250	.1188E7	.3904E8	2,247	.1200E7	.7886E8
148.5	2,125	.1734E7	.1155E9	2,120	.1756E7	.1169E9
195.1	2,000	.2250E7	.1518E9	1,990	.2288E7	.1542E9
239.6	1,875	.2734E7	.1864E9	1,579	.2788E7	.1902E9

Table 3 - Continued

Well D - Average Reservoir Pressure = 5,000 psia

q_g	Without non-Darcy Flow			With non-Darcy Flow		
	p_{wf}	$\bar{p}^2 - p_{wf}^2$	$m(\bar{p}) - m(p_{wf})$	p_{wf}	$\bar{p}^2 - p_{wf}^2$	$m(\bar{p}) - m(p_{wf})$
5,703.6	4,750	.2438E7	.8875E8	4,731	.2616E7	.9548E8
11,435.2	4,500	.4750E7	.1779E9	4,421	.5449E7	.2060E9
17,184.3	4,250	.6938E7	.2674E9	4,067	.8463E7	.3331E9
22,938.4	4,000	.9000E7	.3569E9	3,659	.1161E8	.4785E9
28,679.8	3,750	.1094E8	.4462E9	3,189	.1483E8	.6441E9

Well D - Average Reservoir Pressure = 2,500 psia

q_g	Without non-Darcy Flow			With non-Darcy Flow		
	p_{wf}	$\bar{p}^2 - p_{wf}^2$	$m(\bar{p}) - m(p_{wf})$	p_{wf}	$\bar{p}^2 - p_{wf}^2$	$m(\bar{p}) - m(p_{wf})$
2,545.4	2,375	.6094E6	.3960E8	2,368	.6412E6	.4161E8
5,028.8	2,250	.1188E7	.3904E8	2,222	.1310E7	.8631E8
7,424.2	2,125	.1734E7	.1155E9	2,063	.1995E7	.1336E9
9,755.7	2,000	.2250E7	.1518E9	1,884	.2700E7	.1838E9
11,980.2	1,875	.2734E7	.1864E9	1,686	.3409E7	.2361E9

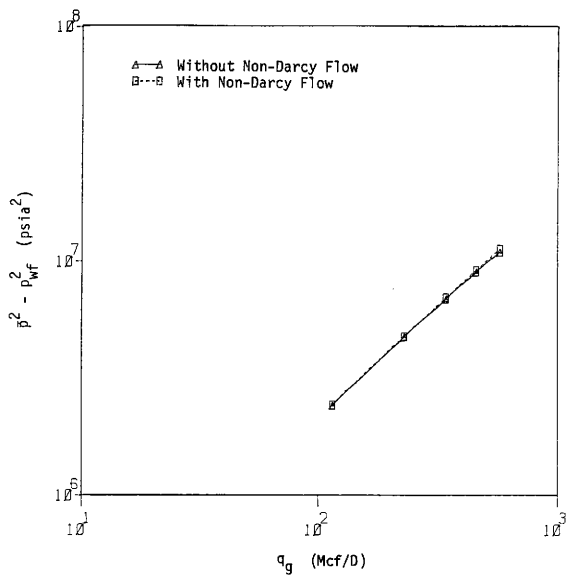


Fig. 19 - Effect of Non-Darcy Flow on Conventional Deliverability Plot
 (Well B, $\bar{p} = 5,000$ psia)

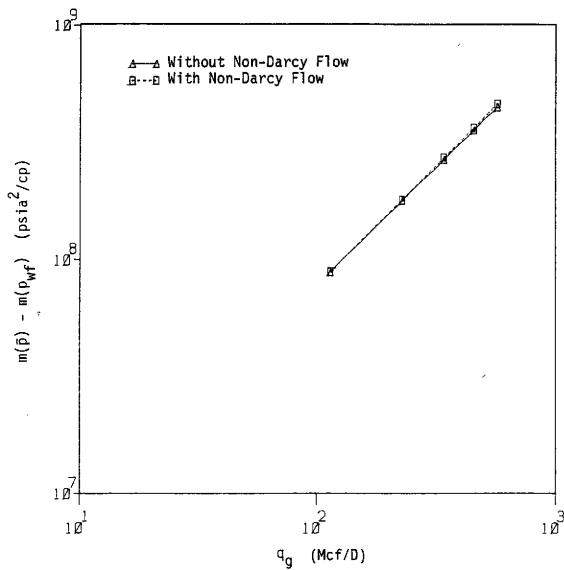


Fig. 20 - Effect of Non-Darcy Flow on Real Gas Pseudo-Pressure Deliverability Plot
 (Well B, $p = 5,000$ psia)

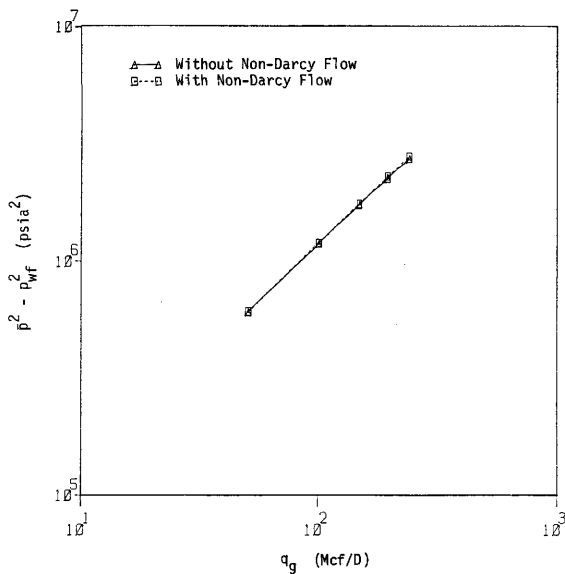


Fig. 21 - Effect of Non-Darcy Flow on Conventional Deliverability Plot
 (Well B, $\bar{p} = 2,500$ psia)

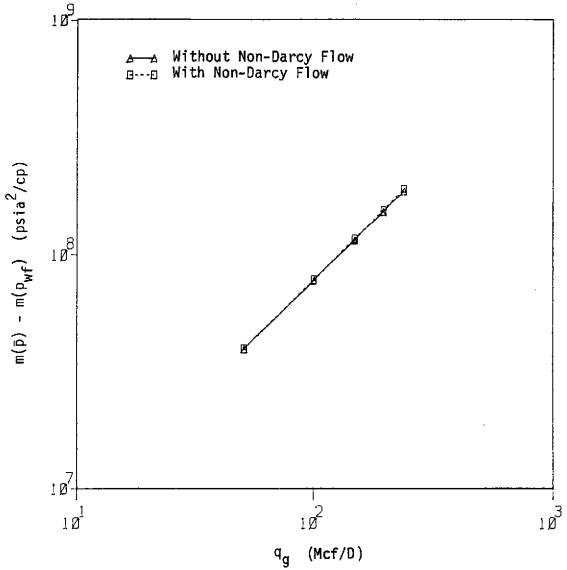


Fig. 22 - Effect of Non-Darcy Flow on Real Gas Pseudo-Pressure Deliverability Plot (Well B, $\bar{p} = 2,500$ psia)

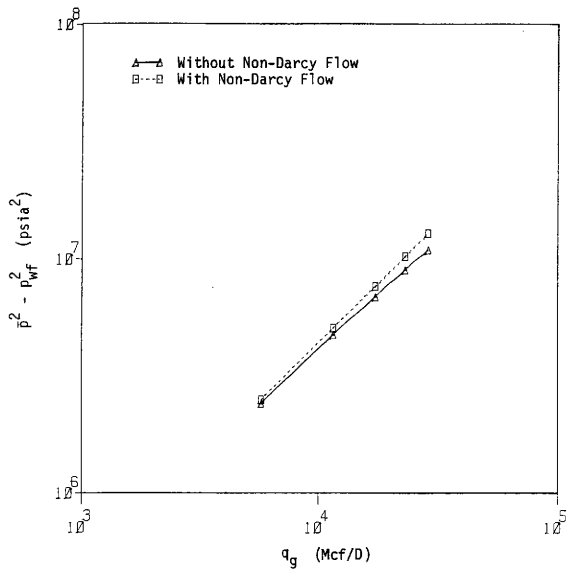


Fig. 23 - Effect of Non-Darcy Flow on Conventional Deliverability Plot
(Well D, $\bar{p} = 5,000$ psia)

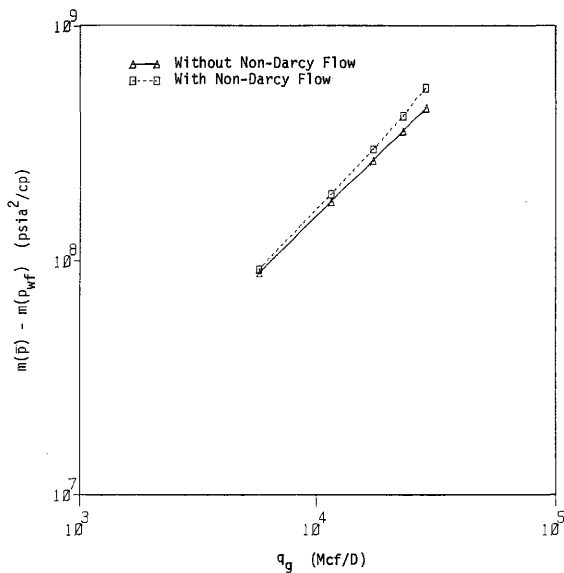


Fig. 24 - Effect of Non-Darcy Flow on Real Gas Pseudo-Pressure Deliverability Plot
 (Well D, $\bar{p} = 5,000$ psia)

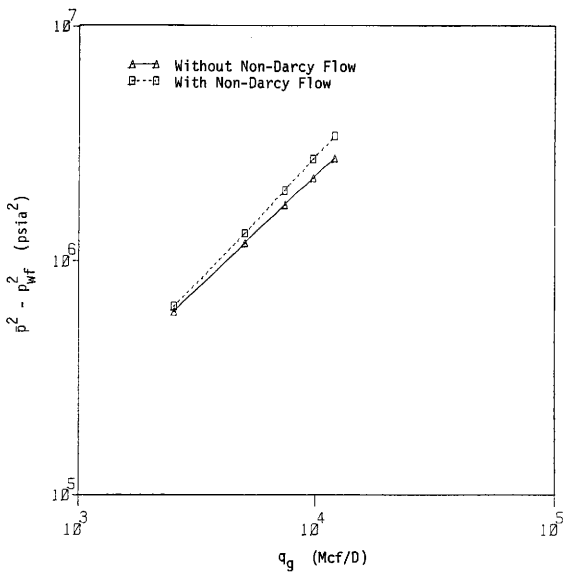


Fig. 25 - Effect of Non-Darcy Flow on Conventional Deliverability Plot
(Well D, $\bar{p} = 2,500$ psia)

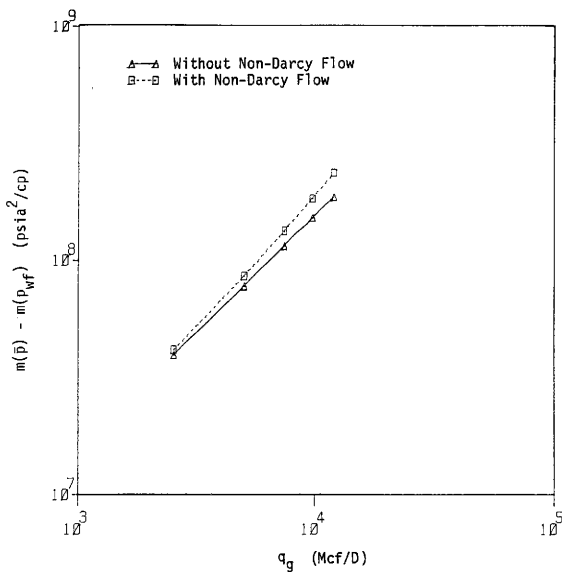


Fig. 26 - Effect of Non-Darcy Flow on Real Gas Pseudo-Pressure Deliverability Plot (Well D, $\bar{p} = 2,500$ psia)

positive skin factor. In gas well testing, non-Darcy flow effects are treated as a dimensionless rate dependent skin factor (seen as $D(\mu)q_g$ in Eqs. 5 and 6). Looking at Eq. 6, the effect of increasing $D(\mu)q_g$ is to increase the value of $\bar{p}^2 - p_{wf}^2$ for a given flow rate. This causes the conventional deliverability plot to bend upward. Eq. 5 also includes the $D(\mu)q$ term, so the $m(p)$ deliverability plot will also bend upward.

It was shown previously that changing gas properties cause deliverability plots from conventional analysis to bend downward if non-Darcy flow effects are negligible. Since changing gas properties and non-Darcy flow effects have opposite effects on the conventional deliverability plot, they will tend to cancel each other out if both are significant. The complex interaction between changing gas properties and non-Darcy flow make it difficult to ascertain the effects of non-Darcy flow alone. Using real gas pseudo-pressure analysis, there are no changing gas property effects. Thus, if bottomhole pressures are calculated correctly, any upward bending of the $m(p)$ deliverability plot can be attributed to non-Darcy flow.

Figs. 19 through 26 confirm the upward bending caused by non-Darcy flow. Since non-Darcy flow is rate dependent, the difference between the deliverability plot with non-Darcy flow and the deliverability plot without non-Darcy flow should be more for high rates. This is confirmed by the deliverability plots for Well D which has high rates. For Well B, which has low rates, non-Darcy flow effects are not

significant and cause only slight upward bending in the deliverability plots.

Note that the $D(u)q$ term is empirical and most likely represents a minimum value of turbulence (i.e., that which would occur if gas were flowing from a homogenous reservoir into a well with an openhole completion). The presence of perforations, partial penetration, a layered system, or inhomogeneities would tend to increase turbulence. Thus, with actual data the deliverability plots may bend upward more severely than illustrated here.

Effects of Bottomhole Pressure Calculation

Before it is possible to use real gas pseudo-pressure analysis to analyze backpressure test data, pressures measured at the surface must be converted to bottomhole pressures. There are several methods available to calculate bottomhole pressures from surface pressures. The methods used here will be the methods described by the RRC²⁵ involving the Weymouth formula and the Cullender and Smith routine.²⁶ Appendix C describes these methods and outlines the calculation techniques. It should be noted that there is no completely reliable method of calculating bottomhole pressures from surface pressures. However, since the Cullender and Smith method is more rigorous than the RRC method, bottomhole pressures calculated using Cullender and Smith will be considered as correct.

To compare the two methods, data from backpressure tests on Wells A, B, C, and D were analyzed using both Cullender and Smith and the RRC method to calculate necessary static and flowing bottomhole pressures. The backpressure test data did not include the effects of non-Darcy flow. Table 4 shows the comparison between bottomhole pressures calculated with the two methods. For Wells A, B, and C the RRC method compares very well to Cullender and Smith especially in terms of percent error. However, for Well D the RRC method breaks down. The reason for the increased error is the the high flow rates associated with Well D. The Weymouth formula used by the RRC overestimates friction pressure drops for high flow rates.

To see the effects of bottomhole pressure on the deliverability plot, the pressures in Table 4 were used to construct the conventional deliverability plots shown in Figs. 27 through 34. For Well A, the deliverability plots from the RRC method are approximately the same as those from Cullender and Smith. For Wells B and C, there is a noticeable difference between the slopes of the deliverability plots from the RRC method and the deliverability plots from Cullender and Smith. This difference is present despite the very small percentage error in calculated bottomhole pressures. Notice that the plots from the RRC method tend to have smaller slopes than the plots from Cullender and Smith. For Well D, the RRC method yields completely unrealistic deliverability plots.

In a conventional deliverability plot, a slope less than one may

Table 4 - Comparison of Bottomhole Pressures Calculated With Cullender and Smith Method and RRC Methods

Well A: Static Wellhead Pressure = 966 psia
 Static Bottomhole Pressure = 1,000 psia (C&S)
 Static Bottomhole Pressure = 1,003 psia (RRC)

q_g (Mcf/D)	P_{wh} (psia)	P_{wf} C&S	P_{wf} RRC	per cent error
14.2	917	950	951	0.10
27.8	870	900	901	0.11
40.7	822	850	851	0.12
53.0	774	800	801	0.13
64.6	726	750	751	0.13

Well A: Static Wellhead Pressure = 485 psia
 Static Bottomhole Pressure = 500 psia (C&S)
 Static Bottomhole Pressure = 501 psia (RRC)

q_g (Mcf/D)	P_{wh} (psia)	P_{wf} C&S	P_{wf} RRC	per cent error
3.9	461	475	475	0.00
7.6	437	450	450	0.00
11.1	412	425	425	0.00
14.5	388	400	400	0.00
17.6	364	375	375	0.00

Table 4 - Continued

Well B: Static Wellhead Pressure = 4,378 psia
 Static Bottomhole Pressure = 5,000 psia (C&S)
 Static Bottomhole Pressure = 5,037 psia (RRC)

q_g (Mcf/D)	P_{wh} (psia)	P_{wf} C&S	P_{wf} RRC	per cent error
114.1	4,131	4,750	4,739	-0.23
228.7	3,900	4,500	4,482	-0.40
343.7	3,669	4,250	4,224	-0.61
458.8	3,439	4,000	3,969	-0.78
573.6	3,212	3,750	3,713	-0.99

Well B: Static Wellhead Pressure = 2,120 psia
 Static Bottomhole Pressure = 2,500 psia (C&S)
 Static Bottomhole Pressure = 2,544 psia (RRC)

q_g (Mcf/D)	P_{wh} (psia)	P_{wf} C&S	P_{wf} RRC	per cent error
50.9	2,008	2,375	2,381	0.25
100.6	1,903	2,250	2,257	0.31
148.5	1,799	2,125	2,133	0.38
195.1	1,694	2,000	2,009	0.45
239.6	1,591	1,875	1,885	0.53

Table 4 - Continued

Well C: Static Wellhead Pressure = 8,832 psia
 Static Bottomhole Pressure = 10,000 psia (C&S)
 Static Bottomhole Pressure = 10,058 psia (RRC)

q_g (Mcf/D)	P_{wh} (psia)	P_{wf} C&S	P_{wf} RRC	per cent error
205.9	8,033	9,500	9,446	0.58
413.9	7,562	9,000	8,920	0.29
624.2	7,093	8,500	8,394	-0.00
836.8	6,627	8,000	7,868	-0.78
1,051.7	6,164	7,500	7,343	-0.83

Well C: Static Wellhead Pressure = 3,941 psia
 Static Bottomhole Pressure = 5,000 psia (C&S)
 Static Bottomhole Pressure = 5,078 psia (RRC)

q_g (Mcf/D)	P_{wh} (psia)	P_{wf} C&S	P_{wf} RRC	per cent error
109.0	3,708	4,750	4,725	-0.53
217.1	3,497	4,500	4,467	-0.73
323.7	3,287	4,250	4,211	-0.92
429.2	3,079	4,000	3,953	-1.18
532.2	2,875	3,750	3,699	-1.36

Table 4 - Continued

Well D: Static Wellhead Pressure = 4,378 psia
 Static Bottomhole Pressure = 5,000 psia (C&S)
 Static Bottomhole Pressure = 5,037 psia (RRC)

q_g (Mcf/D)	p_{wh} (psia)	p_{wf} C&S	p_{wf} RRC	per cent error
5,703.6	4,099	4,750	4,771	0.44
11,435.2	3,765	4,500	4,628	2.84
17,184.3	3,354	4,250	4,587	7.93
22,938.4	2,848	4,000	4,662	16.55
28,679.8	2,198	3,750	4,850	29.33

Well D: Static Wellhead Pressure = 2,120 psia
 Static Bottomhole Pressure = 2,500 psia (C&S)
 Static Bottomhole Pressure = 2,544 psia (RRC)

q_g (Mcf/D)	p_{wh} (psia)	p_{wf} C&S	p_{wf} RRC	per cent error
2,545.0	1,997	2,375	2,398	0.97
5,028.8	1,859	2,250	2,324	3.28
7,424.2	1,697	2,125	2,285	7.52
9,755.8	1,504	2,000	2,278	13.90
11,980.2	1,265	1,875	2,295	22.40

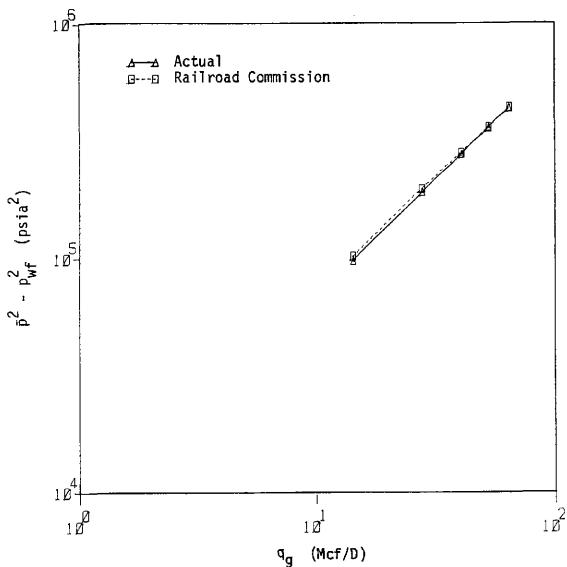


Fig. 27 - Comparison of Backpressure Test Results Using Cullender and Smith Method and RRC Methods to Calculate Bottomhole Pressures (Well A, $\bar{p} = 1,000$ psia, without non-Darcy flow)

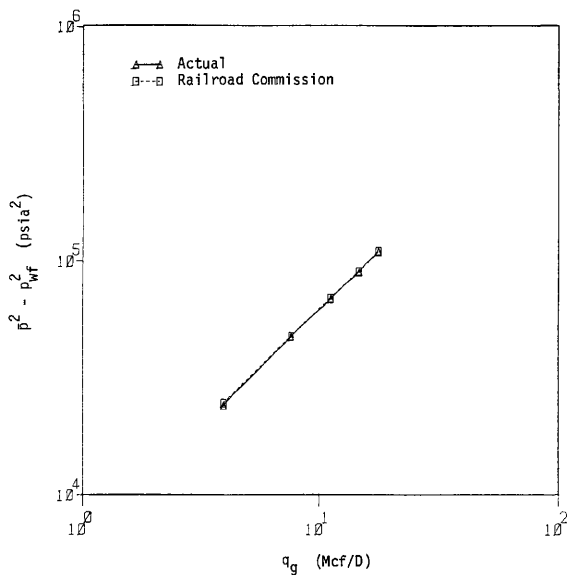


Fig. 28 - Comparison of Backpressure Test Results Using Cullender and Smith Method and RRC Methods to Calculate Bottomhole Pressures (Well A, $\bar{p} = 500$ psia, without non-Darcy flow)

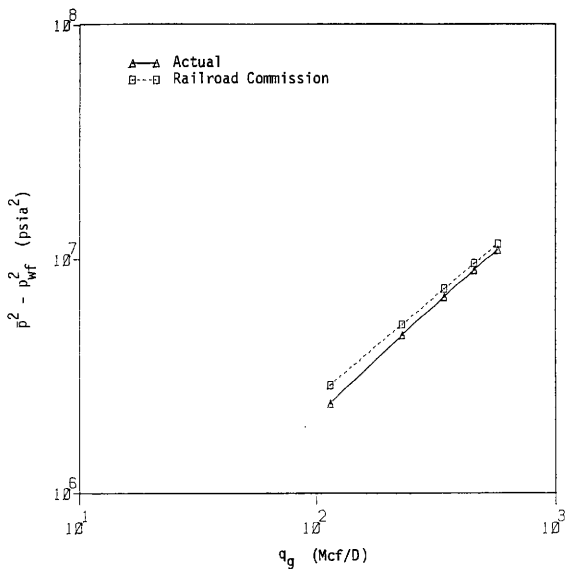


Fig. 29 - Comparison of Backpressure Test Results Using Cullender and Smith Method and RRC Methods to Calculate Bottomhole Pressures (Well B, $\bar{p} = 5,000$ psia, without non-Darcy flow)

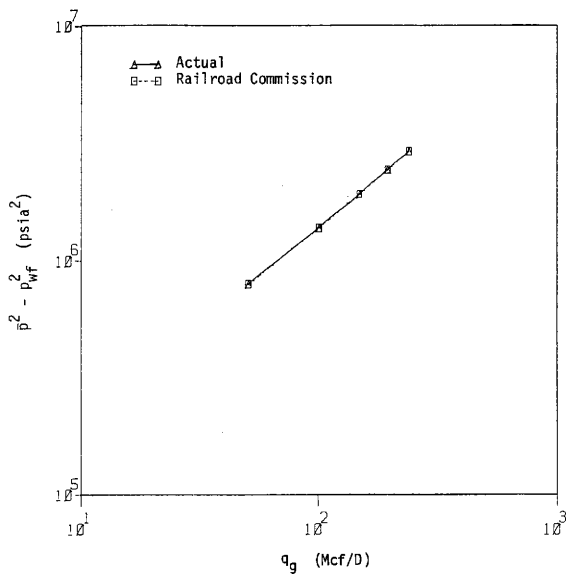


Fig. 30 - Comparison of Backpressure Test Results Using Cullender and Smith Method and RRC Methods to Calculate Bottomhole Pressures (Well B, $\bar{p} = 2,500$ psia, without non-Darcy flow)

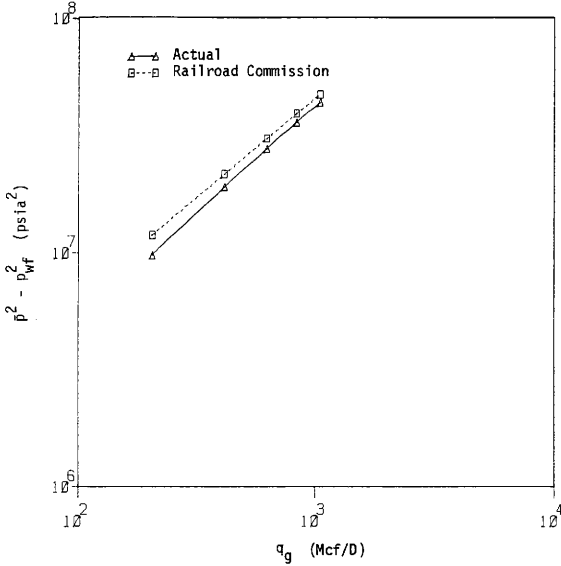


Fig. 31 - Comparison of Backpressure Test Results Using Cullender and Smith Method and RRC Methods to Calculate Bottomhole Pressures (Well C, $p = 10,000$ psia, without non-Darcy flow)

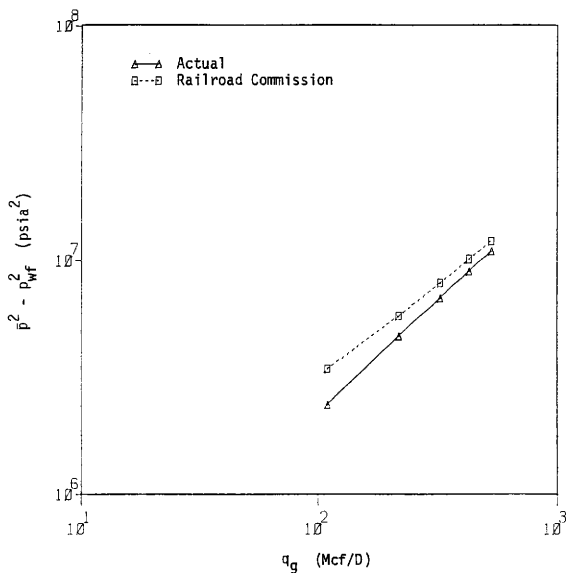


Fig. 32 - Comparison of Backpressure Test Results Using Cullender and Smith Method and RRC Methods to Calculate Bottomhole Pressures (Well C, $\bar{p} = 5,000$ psia, without non-Darcy flow)

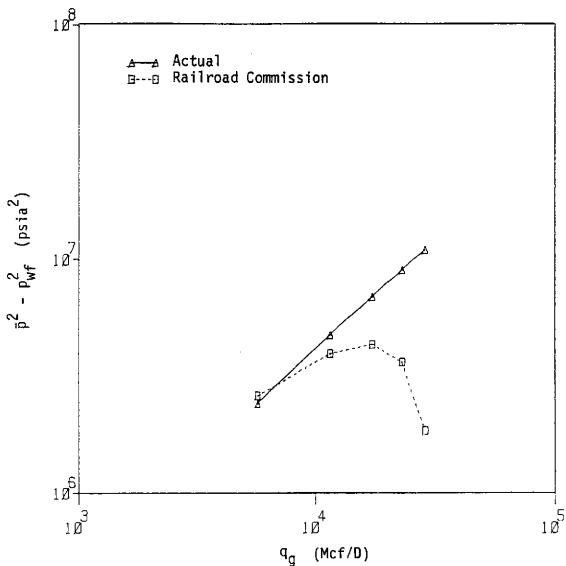


Fig. 33 - Comparison of Backpressure Test Results Using Cullender and Smith Method and RRC Methods to Calculate Bottomhole Pressures (Well D, $\bar{p} = 5,000$ psia, without non-Darcy flow)

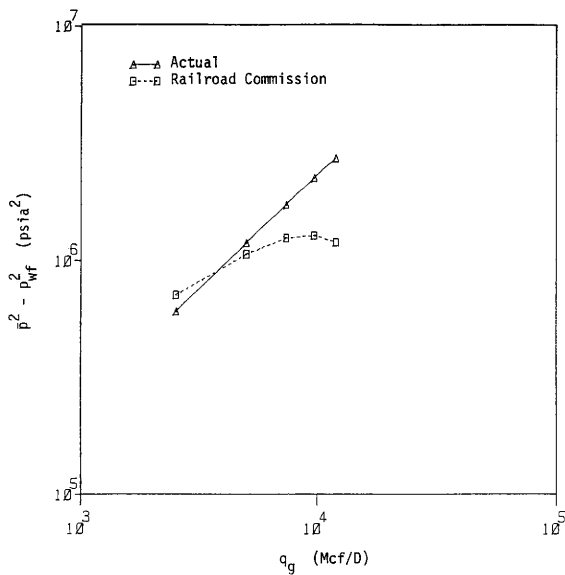


Fig. 34 - Comparison of Backpressure Test Results Using Cullender and Smith Method and RRC Methods to Calculate Bottomhole Pressures (Well D, $\bar{p} = 2,500$ psia, without non-Darcy flow)

be attributed to changing gas properties or incorrect calculation of bottomhole pressures. Using real gas pseudo-pressure accounts for changes in gas properties. Thus, a slope less than one on a $m(p)$ deliverability plot may indicate a miscalculation of bottomhole pressures (due to poor calculation method, incorrect surface pressure data, incorrect temperature data, liquid in the wellbore, etc.).

Forecasting

Previous sections have shown that using real gas pseudo-pressure to analyze backpressure tests removes any bending in the deliverability plot caused by changing gas properties. Since the effects of changing gas properties are eliminated, we would expect a forecast based on the $m(p)$ deliverability plot to be more correct than a forecast based on the conventional deliverability plot. Appendix E describes a simple method of predicting the future productive capacity of a gas well. As explained in the appendix, the method makes use of a material balance plot (\bar{p}/z versus cumulative gas produced), a tubing pressure plot (p_{wf} versus q_g for a constant surface pressure), and a deliverability plot. The deliverability plot may be the conventional deliverability plot, or, preferably, the $m(p)$ deliverability plot. Note that all three plots are based on readily obtainable data and reservoir properties like permeability, porosity, thickness, and area are not needed to make the forecast.

The conventional and $m(p)$ deliverability plots were used to make

forecasts on Wells A, B, C, and D. The forecasts were made using the backpressure test data generated for \bar{p} equal to the initial reservoir pressure. To make the forecasts as realistic as possible, the effects of non-Darcy flow were considered. Figs. 35 through 42 show plots of flow rate versus time and cumulative production versus time for Wells A, B, C, and D.

Examining Figs. 35, 37, 39, and 41 indicates a noticeable difference between flowrate versus time from the two forecasts. For Wells A, B, and D the differences in the forecasts are not real significant considering the simplicity of the forecasting method used. However, for Well C the differences between the forecasts are substantial enough to indicate the possible error in forecasting with the conventional deliverability plot. Further evidence of the possible error in forecasting with the conventional deliverability plot is seen in Figs. 36, 38, 40, and 42. For Wells A, B, and D the difference in cumulative production over the range of the forecast is less than ten percent. For Well C, the difference is over 25 percent. In most reservoir engineering applications, a plus-or-minus ten per cent error is acceptable, but twenty-five per cent is usually not. Thus, high reservoir pressures (greater than 5,000 psia) lead to significant differences between forecasts using the $m(p)$ deliverability plot and forecasts using the conventional plot.

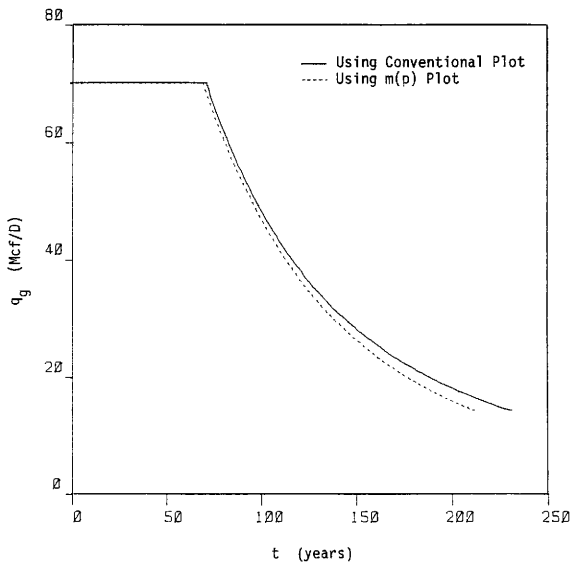


Fig. 35 - Forecast of Rate vs. Time for Well A
(Pipeline pressure = 200 psia)

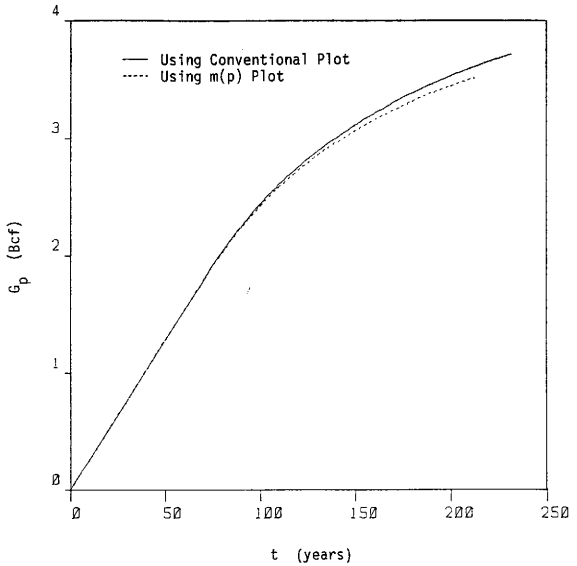


Fig. 36 - Forecast of Cum. Prod. vs. Time for Well A
(Pipeline pressure = 200 psia)

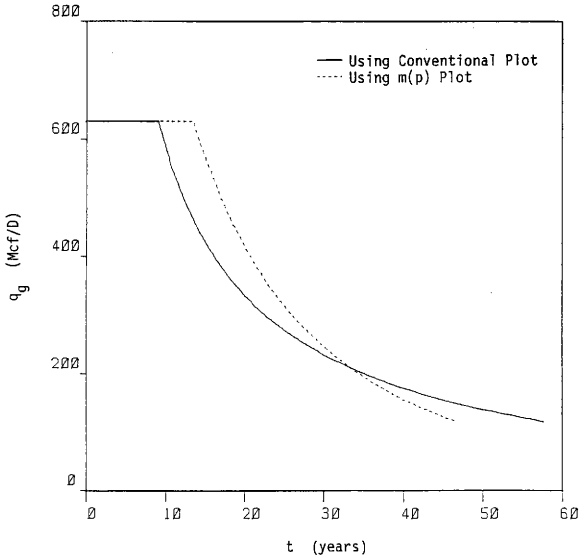


Fig. 37 - Forecast of Rate vs. Time for Well B
(Pipeline pressure = 1,000 psia)

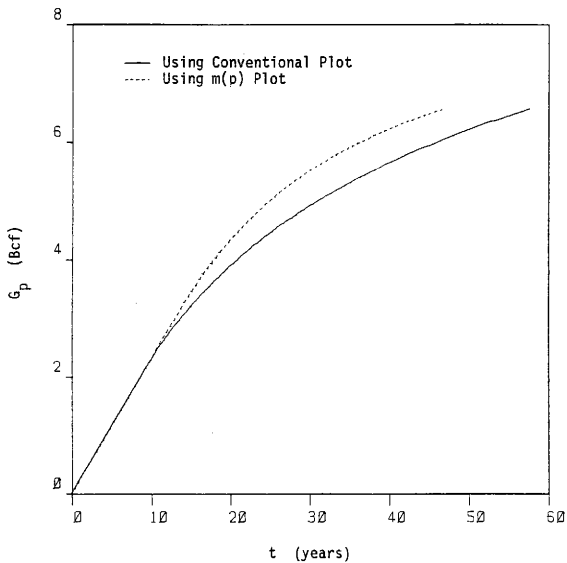


Fig. 38 - Forecast of Cum. Prod. vs. Time for Well B
(Pipeline pressure = 1,000 psia)

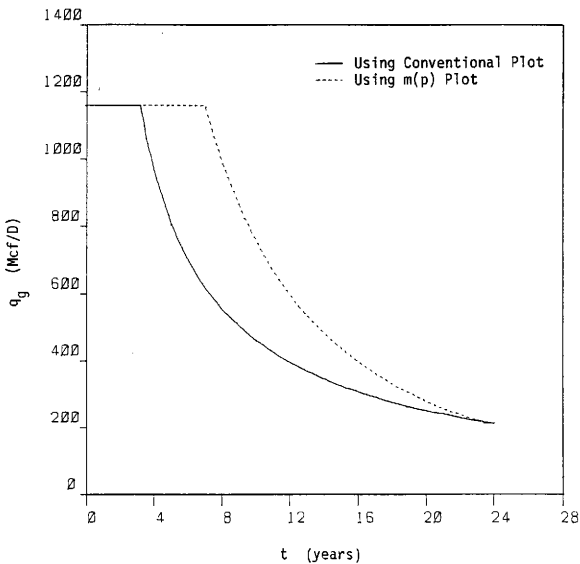


Fig. 39 - Forecast of Rate vs. Time for Well C
(Pipeline pressure = 1,000 psia)

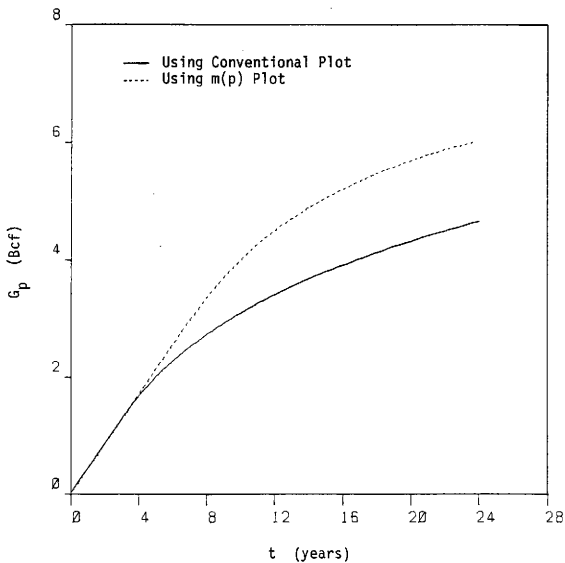


Fig. 40 - Forecast of Cum. Prod. vs. Time for Well C
(Pipeline pressure = 1,000 psia)

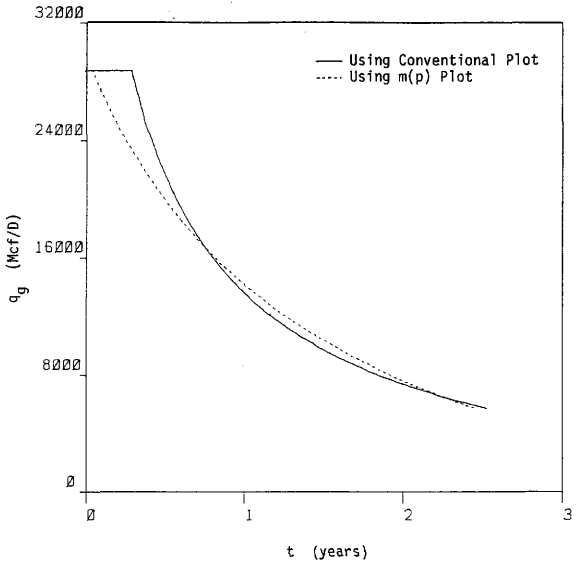


Fig. 41 - Forecast of Rate vs. Time for Well D
(Pipeline pressure = 1,000 psia)

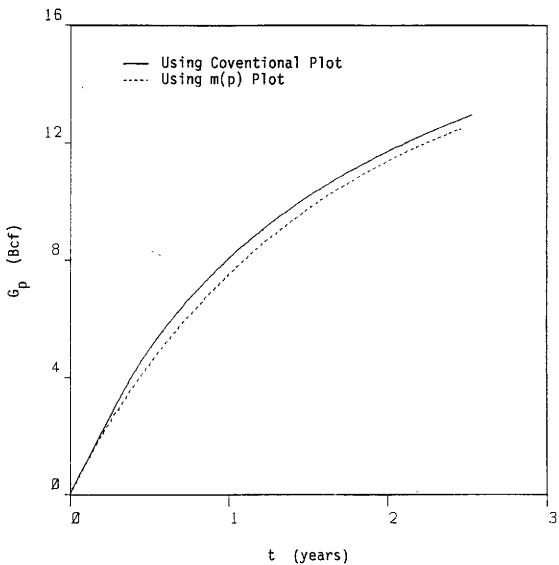


Fig. 42 - Forecast of Cum. Prod. vs. Time for Well D
(Pipeline pressure = 1,000 psia)

DISCUSSION OF RESULTS

The results presented in this research show the effects of changing gas properties, non-Darcy flow, and bottomhole pressure calculations on backpressure tests analysis. Changing gas properties cause the conventional deliverability bend downward. Furthermore, changes in gas properties, due to the depletion of reservoir pressure, cause the conventional deliverability plot to shift positions with time. Both the downward bending and shifting can be removed if real gas pseudo-pressure analysis is used instead of conventional analysis. If non-Darcy flow is negligible, real gas pseudo-pressure analysis results in a single deliverability plot with a unit slope.

The presence of non-Darcy flow causes both the $m(p)$ and conventional deliverability plots to bend upward. However, in the conventional plot, the downward bending caused by changing gas properties tends to lessen the upward bending caused by non-Darcy flow. This can lead to an underestimate of the effects of non-Darcy flow, or possibly, a failure to recognize that non-Darcy flow is occurring. If real gas pseudo-pressure analysis is used, the presence of non-Darcy flow is recognized as an upward deviation from the unit slope line.

The bending caused by changing gas properties and non-Darcy flow become more prevalent as drawdown, and thus rate, increases. To determine the AOF of a gas well, the deliverability plot must be extrapolated through the high rate region where bending is most severe.

Thus, it is doubtful that the straight line drawn through the observed data will extrapolate to the correct AOF. Extrapolation to lower rates can be accomplished with more confidence since both the $m(p)$ and conventional deliverability plots approach a slope of one at lower rates.

Correct interpretation of backpressure tests requires accurate calculation of bottomhole pressures. Unfortunately, such calculations are subject to a wide variety of errors. Even small deviations from the correct bottomhole pressure can cause noticeable differences in the slope of the deliverability plot. One possible clue to the miscalculation of bottomhole pressures is a slope less than one on the $m(p)$ deliverability plot.

Using the forecasting model outlined in Appendix E, it was found that in certain ranges the difference between forecasts using the real gas pseudo-pressure deliverability plot and the conventional plot were not appreciable. Basically, this range consists of wells with pressures less than 5,000 psia. Higher pressures increase the difference between forecast made with $m(p)$ deliverability plots and conventional deliverability plots.

CONCLUSIONS

The results of this research are applicable to data from the pseudosteady-state and steady-state flow regimes and can be summarized with the following conclusions:

1. C in Eq. 1 is a function of z , H , and q_g which are functions of pressure. Thus, for a given backpressure test, C is not a constant.
2. Depletion of reservoir pressure and the resulting changes in gas properties cause the conventional deliverability plot to shift downward with time.
3. For a given backpressure test, changes in p_{wf} and the resulting changes in gas properties cause the conventional deliverability plot to bend downward.
4. The downward bend mentioned above may result in slopes on the conventional deliverability plot that are less than one. The Railroad Commission of Texas, as well as other regulatory bodies, instruct that a slope less than one represents a bad test. However, on a conventional deliverability plot, a slope less than one is possible.
5. Using real gas pseudo-pressure to analyze backpressure tests eliminates the shifting and bending caused by changing gas properties.
6. Non-Darcy flow causes both the $m(p)$ and conventional deliverability plots to bend upward as rate increases.
7. The slope of the deliverability plot is very sensitive

to calculated bottomhole pressures.

8. Using real gas pseudo-pressure analysis results in a deliverability plot with a slope of one if non-Darcy flow is negligible, and a slope greater than one if non-Darcy flow effects are significant. Thus, a $m(p)$ deliverability plot with a slope less than one indicates that calculated bottomhole pressures are wrong.
9. Forecasts made with $m(p)$ deliverability plots and with conventional deliverability plots are not appreciably different for wells with pressures less than 5,000 psia. Higher pressures result in greater and more significant deviations between forecasts made with $m(p)$ deliverability plots and conventional deliverability plots.

NOMENCLATURE

- $a_0 - a_{15}$ = constants for viscosity correlation, Table C1
 C = coefficient describing the position of the stabilized deliverability line, Mcf/psia^2
 c_t = total system compressibility, psia^{-1}
 D = depth to formation, feet
 D_i = turbulent term coefficient, Eq. B2, $(\text{Mcf/D})^{-1}$
 $D(\mu)$ = turbulence coefficient, Eq. B1, $(\text{Mcf/D})^{-1}$
 d_{eff} = effective flow pipe ID, inches
 F = factor for evaluating the effect of gravity in a flowing column of gas, Eq. D7
 F_{CS} = friction pressure term, Eq. D2
 f = friction factor, dimensionless
 G_p = cumulative gas produced, Mcf
 h = thickness of reservoir, feet
 k = permeability, md
 $m(p)$ = real gas pseudo-pressure, Eq. 4, psia^2/cp
 $m(\bar{p})$ = pseudo-pressure evaluated at \bar{p} , psia^2/cp
 $m(p_{\text{wf}})$ = pseudo-pressure evaluated at p_{wf} , psia^2/cp
 n = exponent describing the inverse slope of the stabilized deliverability plot
 p' = dummy variable used in the $m(p)$ integral, psia
 \bar{p} = average reservoir pressure, psia
 P_{avg} = arithmetic mean of \bar{p} and p_{wf} , psia
 P_{fric} = pressure including friction loss, Eq. D6, psia

- p_i = initial reservoir pressure, psia
 p_{pc} = pseudocritical pressure, Eq. C2, psia
 p'_{pc} = corrected pseudocritical pressure, Eq. C8, psia
 p_{pcHC} = pseudocritical pressure of hydrocarbon fraction of gas, Eq. C4, psia
 p_{pr} = pseudo-reduced pressure, p/p_{pc}
 p_{sc} = pressure at standard conditions, psia
 p_{si} = static bottomhole pressure, psia
 p_{wf} = bottomhole flowing pressure, psia
 p_{wh} = wellhead pressure, psia
 q_g = gas flow rate, Mcf/D
 q_{gcap} = maximum flow rate capacity, Mcf/D
 R = friction loss factor, Eq. D5
 r_e = radius to reservoir boundary, feet
 r_w = wellbore radius, feet
 S_g = gas saturation, fraction
 s = skin factor
 T = reservoir temperature, °R
 T_{pc} = pseudocritical temperature, Eq. C1, °R
 T'_{pc} = corrected pseudocritical temperature, Eq. C7, °R
 T_{pcHC} = pseudocritical temperature of hydrocarbon fraction of gas, Eq. C3, °R
 T_{pr} = pseudo-reduced temperature, T/T_{pc}
 T_{sc} = temperature at standard conditions, °R
 T_{wh} = wellhead temperature, °R
 t_{DA} = dimensionless time, Eq. 2

- t_s = time to reach pseudosteady-state, Eq. 3, hours
 y_{CO_2} = mole fraction of carbon dioxide
 y_{H_2S} = mole fraction of hydrogen sulfide
 y_{N_2} = mole fraction of nitrogen
 z = gas law deviation factor, dimensionless

Greek Letters:

- B = turbulence factor, Eq. B3
 C = correction term for gas impurities, Eq. C6, °R
 γ_{gHC} = specific gravity of hydrocarbon portion of gas
 γ_g = specific gravity of gas, air = 1.0
 ϕ = porosity, fraction
 μ = gas viscosity, cp
 μ_i = gas viscosity at initial conditions, cp
 μ_{lam} = gas viscosity for laminar flow conditions, cp
 μ_1 = gas viscosity at atmospheric conditions, Eq. C11, cp

REFERENCES

1. Donohue, D.A.T. and Ertekin, T.: Gaswell Testing: Theory, Practice and Regulation, HRDC Publishers, Boston (1982).
2. Earlougher, R.C.: Advances in Well Test Analysis, Monograph Series, SPE, Dallas (1977) 5.
3. Al-Hussainy, R., Ramey, H.J. Jr., and Crawford, P.B.: "The Flow of Real Gases Through Porous Media," J. Pet. Tech. (May 1966) 624-636.
4. Theory and Practices of the Testing of Gas Wells, Energy Resources Conservation Board, Third Edition, Calgary (1975).
5. Smith, R.V.: Practical Natural Gas Engineering, PennWell Publishers, Tulsa (1983).
6. Pierce, H.R. and Rawlins, E.L.: "The Study of a Fundamental Basis for Controlling and Gauging Natural-Gas Wells. Part 1 - Computing the Pressure at the Sand in a Gas Well," U.S. Bureau of Mines, RI 2929 (1929).
7. Pierce, H.R. and Rawlins, E.L.: "The Study of a Fundamental Basis for Controlling and Gauging Natural-Gas Wells. Part 2 - A Fundamental Relation for Gauging Gas-Well Capacities," U.S. Bureau of Mines, RI 2930 (1929).
8. Rawlins, E.L. and Schellhardt, M.A.: "Back-Pressure Data on Natural Gas Wells and their Application to Production Practices," U.S. Bureau of Mines, Monograph 7 (1935, rev. 1939).
9. "Manual of Back-Pressure Testing of Gas Wells", Interstate Oil Compact Commission, Oklahoma City (1979).
10. Cullender, M.H.: "The Isochronal Performance Method of Determining the Flow Characteristics of Gas Wells," Trans., AIME (1955) 204, 137-142.
11. Cullender, M.H.: "Methods of Determining the Flow Characteristics of Gas Wells," Can. Min. and Met. Bull. (March 1961) 268-271.
12. Govier, G.W.: "Interpretation of the Results of the Back-Pressure Testing of Gas Wells," Can. Min. and Met. Bull. (Dec. 1961) 888-891.
13. Dietz, R. N.: "Determination of Average Reservoir Pressure From Build-Up Surveys," J. Pet. Tech. (Aug. 1965) 955-959.

14. Cornell, D.: "New Method Estimates Gas Well Performance," World Oil (Jan. 1953) 180-184
15. Houpeurt, A.: "Analytical Studies on Transitional Radial Flow of Gas in Porous Media," Revue de L'Institut Francias du Petrole at Annales (1953) 8.
16. Tek, M.R., Grove, M.L., and Poettmann, F.H.: "Method for Predicting the Back-Pressure Behavior of Low Permeability Natural Gas Wells," Trans., AIME (1957) 210, 302-309
17. Carter, R.D., Miller, S.C., and Riley, H.G.: "Determination of Stabilized Gas Well Performance From Short Flow Tests," J. Pet. Tech. (June 1963) 651-658.
18. Riley, H.G.: "A Short Cut to Stabilized Gas Well Productivity," J. Pet. Tech. (May 1970) 537-542.
19. Katz, D.L., Cornell, D., Kobayashi, R., Poettmann, F.H., Vary, J.A., Elenbaas, J.R., and Weinaug, C.F.: Handbook of Natural Gas Engineering, McGraw-Hill Book Co., New York (1959).
20. Wattenbarger, R.A. and Ramey, H.J. Jr.: "Gas Well Testing With Turbulence, Damage, and Wellbore Storage," J. Pet. Tech. (1968) 877-887.
21. Al-Hussainy, R. and Ramey, H.J. Jr.: "Application of Real Gas Flow Theory to Well Testing and Deliverability Forecasting," J. Pet. Tech. (May 1966) 637-642.
22. Wattenbarger, R.A.: "Effects of Turbulence, Wellbore Damage, Wellbore Storage, and Vertical Fractures on Gas Well Testing," PhD Dissertation, Stanford U., Stanford, CA (1967).
23. Aziz, K., Mattar, L., Ko, S., and Brar, G.S.: "Use of Pressure, Pressure Squared, or Pseudo-Pressure in the Analysis of Transient Pressure Drawdown Data from Gas Wells," J. Can. Pet. Tech. (April-June 1976) 58-65.
24. Results from class project, Pet.E. 603, Spring 1985, Texas A&M University, taught by Dr. R.A. Wattenbarger.
25. "Back-Pressure Test for Natural Gas Wells," Railroad Commission of Texas, Austin (1950, reprint 1980).
26. Cullender, M.H. and Smith, R.V.: "Practical Solutions of Gas-Flow Equations for Wells and Pipelines with Large Temperature Gradients," Trans., AIME (1956) 207, 281-287.

27. Firoozabadi, A. and Katz, D.L.: "An Analysis of High-Velocity Gas Flow Through Porous Media," J. Pet. Tech. (Feb. 1979) 211-216.
28. Houpert, A.: "On the Flow of Gases in Porous Media," Revue de L'Institut Francias du Petrole (Nov. 1959) 14, 1468-1684.
29. Standing, M.B.: Volumetric and Phase Behavior of Oil Field Hydrocarbon Systems, SPE, Dallas (1977).
30. Wichert, E. and Aziz, K.: "Calculate z's for Sour Gases," Hydrocarbon Processing (May 1972) 119.
31. Dranchuk, P.M., Purvis, R.A., and Robinson, D.B.: "Computer Calculation of Natural Gas Compressibility Factors Using the Standing and Katz Correlation," Institute of Petroleum Technical Series, No. IP 74-008 (1974).
32. Carr, N.L., Kobayashi, R., and Burrows, D.B.: "Viscosity of Hydrocarbon Gases under Pressure," Trans., AIME (1954) 264-272.
33. Dempsey, J.R.: "Computer Routine Treats Gas Viscosity as a Variable," Oil and Gas J. (Aug. 16, 1965) 141.
34. Aziz, K.: "Calculation of Bottomhole Pressures in Gas Wells," J. Pet. Tech. (July 1967) 897-899.
35. Govier, G.W. and Fogarasi, M.: "Pressure Drop in Wells Producing Gas and Condensate," J. Can. Pet. Tech. (Oct.-Dec. 1975) 28-41.
36. Forecasting method from personal communication with Dr. R. A. Wattenbarger, Texas A&M University, Feb. 1985.

APPENDIX A
PROCEDURE FOR RUNNING BACKPRESSURE TESTS

Basically, backpressure test data consist of a stabilized surface pressure, and several flow rates and their corresponding stabilized surface flowing pressures and temperatures. To run a backpressure test, the following procedure is suggested by the RRC:

- 1) Prior to starting the test, the well should be produced at an average daily rate for a period long enough to reach pseudosteady-state conditions.
- 2) To start the test, the well should be shut in for a sufficient length of time to allow the surface pressure to equalize at some constant value. When converted to bottomhole conditions, the surface pressure read after reaching stabilization is equal to the average reservoir pressure, \bar{p} .
- 3) After the shut-in period, the well should be flowed at a rate sufficient to remove any produced liquids from the wellbore. For gas wells that produce only small amounts of liquid, this rate usually corresponds to a flowing bottomhole pressure equal to approximately 95 per cent of \bar{p} . This rate should be maintained until the surface pressure stabilizes. The flow rate and flowing surface pressure and temperature should be recorded.
- 4) The flow rate is increased and once again maintained until the surface pressure stabilizes. The RRC considers the

reservoir to be stabilized when the surface pressure does not vary more than 0.1 per cent of the original shut-in wellhead pressure during a 15 minute interval. In low permeability reservoirs, this is not a good indication that pseudosteady-state has been achieved.

- 5) At least four different flow rates and their corresponding stabilized flowing surface pressures and temperatures should be taken. If possible, the highest rate should correspond to a flowing bottomhole pressure equal to 75 per cent of \bar{p} .

In addition to the above data, information on well completion and gas properties is also required. As can be seen, backpressure tests are fairly easy to run, although sometimes time consuming. To obtain data that will yield meaningful results, care should be taken to insure that accurate pressure and flowrate measurements are taken, and that these data are taken while the reservoir is in the pseudosteady-state flow regime.

APPENDIX B
GENERATION OF DATA

Data for this research was generated with the real gas pseudosteady-state equation (Eq. 5). For an assumed average reservoir pressure and several flowing bottomhole pressures, the corresponding flow rates were calculated. Average reservoir pressures and flowing bottomhole pressures were converted to surface pressures using the Cullender and Smith²⁶ method. In this way, the flow rate and surface pressure data typically measured in backpressure tests were obtained. Test results could be generated with or without non-Darcy flow. A simple computer program was written to do the necessary calculations.

The effects of non-Darcy flow were calculated using an approximate formula presented by Wattenbarger and Ramey:²⁰

$$D(u) = D_i \frac{\mu_i}{\mu_{iam}} \quad (B1)$$

where

$$D_i = \frac{2.2229 \times 10^{-15} \beta_{yg} k}{\mu_i h r_w} \quad (B2)$$

In both Eqs. B1 and B2, μ_i is taken at the average reservoir pressure used in the backpressure test calculations. The μ_{iam} term is the viscosity taken at the flowing bottomhole pressure that would

occur if non-Darcy flow effects were not present. The β term in Eq. B2 is called the velocity coefficient or turbulence factor. By flowing gas through core samples it was possible to correlate β to rock properties. Several correlations exist,²⁷ but in this research the correlation of Houpeurt²⁸ was used:

$$\beta = 2.234794 \times 10^{-10} k^{-1.201} \quad (B3)$$

To generate backpressure test data including non-Darcy flow effects, average reservoir pressure and flowing bottomhole pressure are once again assumed. The corresponding flow rate is calculated using Eq. 5 with the $D(\mu)$ term set to zero. The laminar viscosity, μ_{lam} , is calculated at the assumed flowing bottomhole pressure, and μ_i is calculated at the average reservoir pressure. With these viscosities, it is possible to calculate $D(\mu)$. A new flowing bottomhole pressure including non-Darcy flow can then be calculated by rearranging Eq. 5 as:

$$m(p_{wf}) = m(\bar{p}) - q_g \left[\frac{\left(\frac{p_{sc} T}{T_{sc}} \right) \ln \left(\frac{0.472 r_e}{r_w} + s + D(\mu) q_g \right)}{1.987 \times 10^{-5} kh} \right] \quad (B4)$$

APPENDIX C
CORRELATIONS FOR GAS PROPERTIES

To generate the data used in this research it was necessary to know gas properties as functions of temperature and pressure. The gas properties, specifically viscosities and z-factors, were needed to generate real gas pseudo-pressures using Eq. 4 and in the Cullender and Smith bottomhole pressure routine. There are several correlations available for various gas properties. The ones used in this research were chosen based on accuracy and adaptability to computer programs.

The following correlation was used to calculate the pseudocritical temperature and pressure of the gas:²⁹

$$T_{pc} = (1 - y_{N_2} - y_{CO_2} - y_{H_2S})T_{pcHC} + 227y_{N_2} + 548y_{CO_2} + 672y_{H_2S} \quad (C1)$$

$$p_{pc} = (1 - y_{N_2} - y_{CO_2} - y_{H_2S})p_{pcHC} + 493y_{N_2} + 1071y_{CO_2} + 1306y_{H_2S} \quad (C2)$$

where

$$T_{pcHC} = 170.491 + 307.344y_{gHC} \quad (C3)$$

$$p_{pcHC} = 709.604 - 58.718y_{gHC} \quad (C4)$$

and

$$Y_{gHC} = \frac{Y_g - 0.967y_{N_2} - 1.52y_{CO_2} - 1.18y_{H_2S}}{1 - y_{N_2} - y_{CO_2} - y_{H_2S}} \quad (C5)$$

The pseudocritical properties from Eqs. C1 and C2 can be corrected for the presence of carbon dioxide, hydrogen sulfide, and nitrogen using the method of Wichert and Aziz:³⁰

$$\epsilon = 120 \left[(y_{CO_2} + y_{H_2S})^{0.9} - (y_{CO_2} + y_{H_2S})^{1.6} \right] + 15 (y_{CO_2}^{0.5} - y_{H_2S}^4) \quad (C6)$$

$$T_{pc}^i = T_{pc} - \epsilon \quad (C7)$$

$$p_{pc}^i = \frac{p_{pc} (T_{pc} - \epsilon)}{T_{pc} + y_{H_2S} (1 - y_{H_2S}) \epsilon} \quad (C8)$$

Compressibility factors were calculated using an eight parameter Benedict-Webb-Rubin equation of state developed by Dranchuk, Purvis, and Robinson.³¹ This method effectively reproduces the Standing and Katz z-factor charts. The ERCB manual on gas well testing⁴ presents a subroutine to do the necessary calculations and iterations. This subroutine was used to calculate the required z-factors.

Gas viscosity was determined using the correlation of Carr,

Kobayashi, and Burrows.³² This correlation was adapted to the computer by Dempsey.³³ The basic equation is:

$$\ln\left(\frac{\mu}{\mu_1} T_{pr}\right) = a_0 + a_1 p_{pr} + a_2 p_{pr}^2 + a_3 p_{pr}^3 \\ + T_{pr}(a_4 + a_5 p_{pr} + a_6 p_{pr}^2 + a_7 p_{pr}^3) \\ + T_{pr}^2(a_8 + a_9 p_{pr} + a_{10} p_{pr}^2 + a_{11} p_{pr}^3) \\ + T_{pr}^3(a_{12} + a_{13} p_{pr} + a_{14} p_{pr}^2 + a_{15} p_{pr}^3) \quad (C9)$$

where

$$\mu_1 = (\mu_1 \text{ uncorrected}) + (N_2 \text{ correction}) \\ + (CO_2 \text{ correction}) + (H_2S \text{ correction}) \quad (C10)$$

and

$$(\mu_1 \text{ uncorrected}) = (1.709 \times 10^{-5} - 2.6062 \times 10^{-6} \gamma_g)T \\ + 8.188 \times 10^{-3} - 6.15 \times 10^{-3} \log(\gamma_g) \quad (C11)$$

$$(N_2 \text{ correction}) = y_{N_2}(8.48 \times 10^{-3} \log(\gamma_g) + 9.59 \times 10^{-3}) \quad (C12)$$

$$(CO_2 \text{ correction}) = y_{CO_2}(9.08 \times 10^{-3} \log(\gamma_g) + 6.24 \times 10^{-3}) \quad (C13)$$

$$(H_2S \text{ correction}) = y_{H_2S}(8.49 \times 10^{-3} \log(\gamma_g) + 3.73 \times 10^{-3}) \quad (C14)$$

Eq. C9 can be solved for μ , the viscosity of the gas at the desired temperature and pressure. The 'a' constants used in Eq. C9 are given in Table C1.

Table C1 - Constants for Viscosity Correlation

a_0	=	-2.46211820E-00
a_1	=	2.97054714E-00
a_2	=	-2.86264054E-01
a_3	=	8.05420522E-03
a_4	=	2.80860949E-00
a_5	=	-3.49803305E-00
a_6	=	3.60373020E-01
a_7	=	-1.04432413E-02
a_8	=	-7.93385684E-01
a_9	=	1.39643306E-00
a_{10}	=	-1.49144925E-01
a_{11}	=	4.41015512E-03
a_{12}	=	8.39387178E-02
a_{13}	=	-1.86408848E-01
a_{14}	=	2.03367881E-02
a_{15}	=	-6.09579263E-04

APPENDIX D
BOTTOMHOLE PRESSURE CALCULATIONS

Because of the expense involved in directly measuring bottomhole pressures, most backpressure tests will have data consisting only of pressures measured at the surface. This necessitates the use of some method to convert surface pressures to their corresponding bottomhole pressures. The method used in this research to generate data and analyze backpressure tests was the Cullender and Smith²⁶ routine. This method is applicable to a wide range of producing conditions and is easily adaptable to the computer.

The equations presented by Cullender and Smith are, for the static bottomhole pressure calculation,

$$\frac{\gamma_g D}{53.34} = \int_{p_{si}}^{p_{wh}} \frac{Tz}{p} dp \quad (D1)$$

and for the flowing bottomhole pressure calculation,

$$\frac{1000\gamma_g D}{53.34} = \int_{p_{wf}}^{p_{wh}} \frac{\left(\frac{p}{Tz}\right)}{F_{cs}^2 + \left(\frac{p}{1000}\right)^2} dp \quad (D2)$$

where

$$F_{cs} = \frac{2.6665fq^2}{d_{eff}} \quad (D3)$$

The calculation procedure is:

- 1) Assume a value of p_{wh} .
- 2) Compute the right-hand side of Eq. D1 or D2 depending on the type of calculation being done (static or flowing).
- 3) Compare the computed value of the integral to the known left-hand side of the equation. If the two sides are not equal within a certain tolerance, the calculations are repeated with a new estimate of p_{wh} .

Aziz³⁴ presented a method involving a Newton-Raphson iteration scheme to reduce the number of iterations required for convergence. This scheme was incorporated into computer program for calculating bottomhole pressures.

Another method of calculating bottomhole pressures is by using the Weymouth formula as presented in the Railroad Commission (RRC) manual.²⁵ The Weymouth formula was originally derived for pipeline flow and later modified for wellbore flow. The formula uses average gas properties and assumes a small temperature gradient.

To calculate the static bottomhole pressure, p_{sj} , the following procedure is used:

- 1) Assume a value of p_{sj} .
- 2) Calculate the z-factor at average temperature and pressure where $T_{avg} = \frac{1}{2}(T_{wh} + T)$ and $p_{avg} = \frac{1}{2}(p_{wh} + p_{sj})$.
- 3) Calculate a new value of p_{sj} .

$$p_{si} = p_{wh} e^{\left(\frac{\gamma_g D}{53.34 T_{avg} z} \right)} \quad (04)$$

- 4) If the calculated value of p_{si} does not equal the assumed value, the calculated value is used as the new assumed value and the calculations are repeated.

To calculate the flowing bottomhole pressure, p_{wf} , the following procedure is used:

- 1) Calculate the friction loss factor,

$$R = \frac{q_g \sqrt{\gamma_g D T_{avg}}}{1118 d_{eff}^{2/3}} \quad (05)$$

- 2) Calculate the pressure resulting from friction losses,

$$p_{fric} = \sqrt{p_{wh}^2 + R^2} \quad (06)$$

- 3) Calculate F, a factor for evaluating the effect of gravity in a flowing column of gas,

$$F = 0.6667 \left[1 + \frac{p_{wh}/p_{fric} - \frac{p_{wh}/p_{fric}}{1 + p_{wh}/p_{fric}} \right] \quad (07)$$

- 4) Calculate the flowing bottomhole pressure,

$$p_{wf} = p_{fric} e^{\left(\frac{\gamma_g D F}{53.34 T_{avg} z} \right)} \quad (08)$$

The Weymouth formula works best in low pressure, low temperature, low flow rate wells. High rates result in calculated values of R , and subsequently p_{wf} , that are too large. In general, the Weymouth formula is not as reliable as Cullender and Smith and should not be used. Both methods are applicable only to dry gas or low liquid rate wells. If high liquid rates are present, other methods should be used.³⁵

APPENDIX E

FORECASTING PROCEDURE

The prediction of the future productive capacity of a well is essential for economic evaluations and reservoir management. If sufficient time, money, and data are available, reservoir simulation techniques can be used to obtain the best possible prediction of gas well performance. Unfortunately, time, money, and data are frequently not available, so less sophisticated methods of estimating future performance must be employed. One such method³⁶ requires only a tubing pressure plot, a stabilized deliverability plot, and a material balance plot. The tubing pressure plot relates flowing bottomhole pressure to flow rate assuming surface pressure is equal to a relatively constant pipeline or separator pressure. The material balance plot is usually the standard \bar{p}/z plot. The stabilized deliverability plot relates average reservoir pressure, flowing bottomhole pressure, and flow rate. Figs. E1, E2, and E3 show examples of a tubing pressure plot, deliverability plot and material balance plot necessary to make a forecast.

For purposes of forecasting gas production it is convenient to assume that C and n of Eq. 1 remain constant throughout the life of the well. However, declining reservoir pressure and the resulting changes in gas properties cause the deliverability plot to shift with time. Thus, predictions of gas well performance utilizing the assumption of

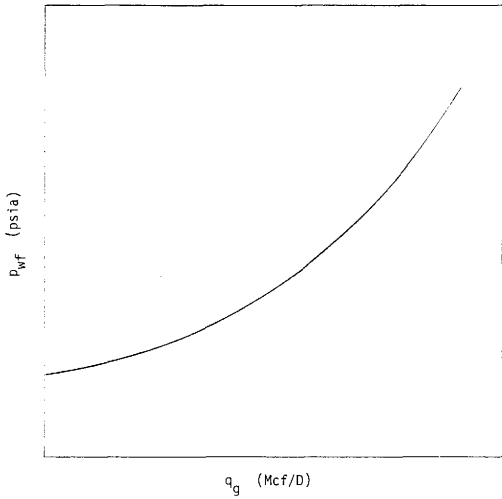


Fig. E1 - Tubing Pressure Plot Used to Make Forecast

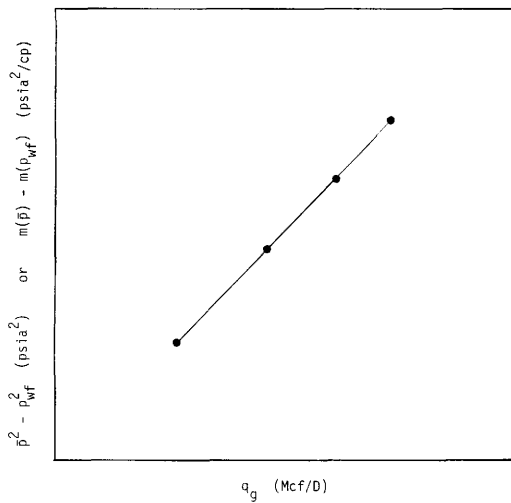


Fig. E2 - Deliverability Plot Used to Make Forecast

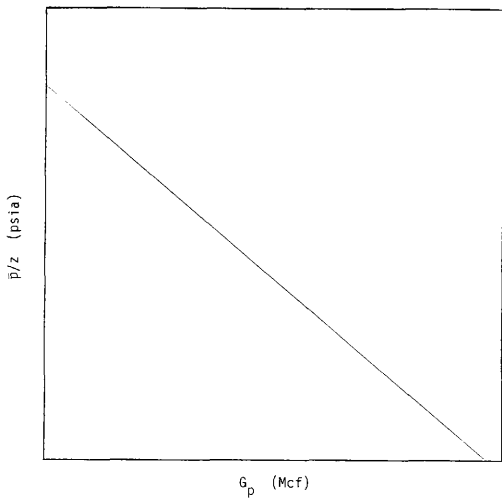


Fig. E3 - Material Balance Plot Used to Make Forecast

constant C and n may lead to significant errors. Using real gas pseudo-pressure analysis of backpressure tests removes the effects of changing gas properties. Because of this, a forecast based on a real gas pseudo-pressure representation of the deliverability plot will yield better estimates of future gas well performance than assuming constant C and n .

The following steps outline a simple forecasting technique for obtaining the maximum flow rate capacity, q_{gcap} , of a gas well versus time.

- 1) Plot \bar{p}/z versus G_p to get the material balance plot.
- 2) Calculate an appropriate tubing curve using the Cullender and Smith method, assuming constant surface pressure.
- 3) Analyze the backpressure test data using real gas pseudo-pressures to get the deliverability plot.
- 4) Develop points on a q_{gcap} -versus G_p curve as follows.
 - a) For several values of q_{gcap} , read p_{wf} from the tubing curve.
 - b) For given q_{gcap} and p_{wf} , find corresponding \bar{p} from the $m(p)$ deliverability plot.
 - c) Find z corresponding to \bar{p} and read G_p from material balance plot.
 - d) Plot q_{gcap} versus G_p (smooth curve if necessary).
- 5) Take successive increments of G_p (G_{p1} , G_{p2} ...).
 - a) Calculate average rate $q_{avgi} = \frac{1}{2}(q_{gcap i} + q_{gcap i-1})$.
 - b) Calculate $t_i - t_{i-1} = (G_{pi} - G_{pi-1})/q_{avgi}$.

- c) From the material balance plot, find values of \bar{p}_i for all G_{pi} .
- d) Plot G_{pi} , q_{gcapi} , and \bar{p}_i versus Σt_i .

The above procedure requires a number of repetitive calculations, therefore, a computer program was written to assist in developing the forecast. This simple forecasting method is by no means rigorous, yet it provides a quick, inexpensive approximation of the future performance of the well. Also, the method has the advantage that reservoir properties like permeability, porosity, thickness, and area are not required to make the forecast.

VITA

Name: Thomas Gary Corbett

Born: September 22, 1960
Houston, Texas

Parents Mr. and Mrs. Thomas S. Corbett

Permanent Address: P. O. Box 2771
Conroe, Texas 77305

University: The University of Texas
Austin, Texas
Bachelor of Science Degree in
Petroleum Engineering (August 1983)

Texas A&M University
College Station, Texas
Master of Science Degree in
Petroleum Engineering (August 1985)

Member: Society of Petroleum Engineers of AIME
Pi Epsilon Tau